Nonlinear Anal. RWA 77 (2024) 104042

Contents lists available at ScienceDirect

Nonlinear Analysis: Real World Applications

journal homepage: www.elsevier.com/locate/nonrwa

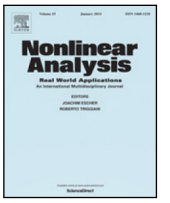

A domain-dependent stability analysis of reaction–diffusion systems with linear cross-diffusion on circular domains

Gulsemay Yigit [a], Wakil Sarfaraz [b], Raquel Barreira [c,d], Anotida Madzvamuse [e,f,g,*]

[a] Department of Mathematics, Faculty of Engineering and Natural Sciences, Bahcesehir University, Istanbul, Turkey
[b] Professional Development Expert (PDE), Corndel Ltd., 410 Highgate Studio 53-79 Highgate Road, London NW5 1TL, United Kingdom
[c] Instituto Politécnico de Setúbal, Escola Superior de Tecnologia do Barreiro, Rua Américo da Silva Marinho-Lavradio 2839-001 Barreiro, Portugal
[d] Centro de Matemática, Aplicações Fundamentais e Investigação Operacional (CMAFcIO), Universidade de Lisboa, Portugal
[e] Mathematics Department, The University of British Columbia, Mathematics Building, 1984 Mathematics Road, Vancouver, BC Canada V6T 1Z2
[f] Department of Mathematics and Applied Mathematics, University of Pretoria, Pretoria 0132, South Africa
[g] Department of Mathematics and Applied Mathematics, University of Johannesburg, PO Box 524 Auckland Park, 2006, South Africa

ARTICLE INFO

Keywords:
Reaction–cross–diffusion systems
Domain-dependent instability
Cross-diffusion-driven instability
Pattern formation
Spatiotemporal dynamics
Circular disc domains

ABSTRACT

In this study, we present theoretical considerations of, and analyse, the effects of circular geometry on the stability analysis of semi-linear parabolic PDEs of reaction–diffusion type with linear cross-diffusion for a two-component system on circular domains. The highlights of our theoretical and computational findings are: (i) By employing linear stability analysis for a two-component reaction–diffusion system with linear cross-diffusion on circular disc domains, we derive necessary and sufficient conditions for the system to exhibit cross-diffusion driven-instability, dependent on the length scale of the geometry. These analytical studies involve cross-diffusion and circular geometry to unravel analytical conditions for the full computational classification of the parameter spaces that allow the system to exhibit Turing, Hopf and transcritical patterns. (ii) We compute parameter spaces on which patterns are formed only due to linear cross-diffusion as well as due to a critical domain length. These spaces do not exist in the absence of cross-diffusion nor when the conditions on the domain length are violated. (iii) To support our theoretical findings, finite element simulations illustrating the formation of spot patterns on circular domains are presented. Model parameter values are selected from parameter spaces that are induced by cross-diffusion, thereby supporting linear cross-diffusion coupled with reaction–diffusion theory as a candidate mechanism for pattern formation. (iv) A by-product of this study, is that an activator-depleted reaction–diffusion system with linear cross-diffusion on circular domains, appears to favour the formation of spot patterns for most of the parameter values chosen. Such patterns are reminiscent of those observed on stingrays, which form on approximately circular domains during growth development.

* Corresponding author at: Mathematics Department, The University of British Columbia, Mathematics Building, 1984 Mathematics Road, Vancouver, BC Canada V6T 1Z2 .
E-mail address: am823@math.ubc.ca (A. Madzvamuse).

https://doi.org/10.1016/j.nonrwa.2023.104042
Received 10 July 2023; Received in revised form 5 November 2023; Accepted 13 November 2023
Available online 20 November 2023

1. Introduction

Reaction–diffusion equations have attracted a lot of attention due to the wide variety of applications ranging from the formation of patterns in animal skins to the growth of embryonic structures [1–6]. A renowned scientist Alan Turing first proposed a significant theory on pattern formation in nature in his seminal article in 1952 [7]. Turing's theory points out how self-organized pattern formation emerges from the interactions on reaction and diffusion of multi-component systems in many biological processes [8–10]. Despite its far reaching impact, the theory has significant limitations. One such limitation is the fact that, for a two component reaction diffusion system, for example, equal diffusion coefficients cannot give rise to patterning. Nevertheless, reaction–diffusion systems (RDS), including activator-depleted kinetics that describes dynamics of the two species, has been widely used in understanding the spatially periodic structure of Turing patterns [10–17].

Cross-diffusion refers to a phenomenon where the concentration gradient of one species is affected by the fluxes of other species in biological and chemical systems. Reaction–diffusion systems without cross-diffusion accepts that diffusion of one species is independent from the concentration gradients of other species, hence only a self-diffusion process is described. In addition, the emergence of pattern formation in classical reaction–diffusion systems without cross-diffusion requires that the diffusion rate of the inhibitor has to be much larger than the diffusion rate of the activator. This limitation is overcome by the addition of cross-diffusion to the system, which entails that the inclusion of long-range inhibition and short-range activation is no longer a necessary condition for pattern formation under Turing's diffusion-driven instability theory [8,9,11,12,18]. Reaction–diffusion systems with linear cross-diffusion have been proposed in understanding the dynamics of a wide range of biological and chemical process. It has also been shown that the existence of cross-diffusion in the reaction–diffusion systems has significant effect on the evolution of spatial pattern formation [8,12,18]. Cross-diffusion induced reaction–diffusion systems have been widely studied in understanding the complex dynamical behaviour of biological processes. Studies on [11,12] revealed Turing type of diffusion-driven instability conditions for the reaction–diffusion system with cross-diffusion on stationary and growing domains. In [11,12] unstable regions satisfying these conditions have been presented for the spatial patterns supported by numerical simulations. In addition to spatial pattern formation, our contribution includes the conditions for understanding the spatiotemporal dynamics of the reaction–diffusion systems in the presence of cross-diffusion. More recent researches include prey–predator systems [19–22], pattern formation [23–28], bacterial chemotaxis [29–31], as well as epidemic models [32–35] and so forth. Another application of RDEs where the presence of cross-diffusion is relevant and backed up experimentally is given by electrodeposition [36]. A recent study on reaction–diffusion [27] systems exhibiting the cross-diffusion provides spatiotemporal pattern formation and numerical simulations considering the effects of different initial conditions on the stationary rectangular domains. Comparing our contribution with the study [27], our results reveal the influence of the domain-size on the spatiotemporal pattern formation with the conditions which are essential on the circular geometries.

The spatiotemporal dynamics of the RDSs are closely related to the domain-size of the model. The main reason behind this mechanism is that the domain of the model must have a certain size for the patterns to be evolved [12,13,15–17,37]. To contextualize this study with regards to current state-of-the-art analysis on the criticality of the domain length, it must be noted that it is known in the literature that when the domain size is *large enough to allow for the formation of patterns, but also small enough to affect pattern selection*, the so-called *intrinsic patterns* arise. This is true on both flat domains [38] and surfaces [39]. All of these results are qualitative. The present paper finally gives a quantitative understanding to these results for the case of circular domains.

Numerical approaches are useful to study such dynamical behaviour of the activator-depleted models due to the existence of the nonlinear reaction kinetics. The finite element method is one of the popular numerical techniques for obtaining a numerical solution of differential equations. It is flexible with working on different kind of geometries with proper boundary conditions and numerous studies have investigated RDs using numerical methods and developed various techniques to understand dynamical behaviour on different geometries [40–44]. We have used it to enable visualization of the type of pattern structures that result from the different types of instabilities.

In this article, we aim to study the influence of the domain size on the spatiotemporal pattern formation of the cross-diffusive RDs in polar coordinates. We generalize the framework presented in [16] by extending the results to include the cross-diffusion parameters on disc-shape domain. We also explore the classification of unstable parameter regions in the presence of cross-diffusion on the given domain. The process of generation of the parameter spaces for the classification of the unstable spaces is accomplished through the detailed investigation of the stability matrix which is obtained with the help of linear stability analysis. Regions corresponding to the unstable spaces can be understood by the eigenvalues of the stability matrix. The solution of the eigenvalue problem satisfying the boundary conditions is one of the key concept in the process of linearization. We use the analytical results of eigenvalue problem to obtain the stability matrix which is necessary to present the system parameters.

The rest of the article is structured as follows. In the following section, we give the details of the activator-depleted model with cross-diffusion terms in polar coordinates. In Section 2, we present the results of analytical approach based on linear stability analysis. In addition, conditions of spatial and spatiotemporal pattern formation are presented with proofs. In Section 3, we present the parameter spaces with a detailed classification varying the system parameters d, d_u, d_v and γ in light of the conditions derived in Section 2. In Section 4, we provide finite element solutions of the model on the two-dimensional disc-shape domain to verify the analytical findings based on the conditions given by Theorems 2, 3 and 5. In Section 5, we present conclusive remarks and future directions of the work.

1.1. Model equations

We consider a non-dimensionalized reaction–diffusion system (RDS) with linear cross diffusion for two chemical species $u(r,\theta,t)$ and $v(r,\theta,t)$ with homogeneous Neumann boundary conditions given by

$$\begin{cases} \begin{cases} \dfrac{\partial u}{\partial t} = \Delta_r u + d_v \Delta_r v + \gamma f(u,v), \\ \dfrac{\partial v}{\partial t} = d\,\Delta_r v + d_u \Delta_r u + \gamma g(u,v), \end{cases} & (r,\theta) \in \Omega,\ t > 0, \\ \dfrac{\partial u}{\partial r} + d_v \dfrac{\partial v}{\partial r} = d_u \dfrac{\partial u}{\partial r} + d \dfrac{\partial v}{\partial r} = 0,\ (r,\theta) \in \partial\Omega,\ t \geq 0, \\ u(r,\theta,0) = u_0(r,\theta),\ v(r,\theta,0) = v_0(r,\theta),\ (r,\theta) \in \Omega,\ t = 0, \end{cases} \tag{1}$$

where d and γ are positive real constants. In system (1), Δ_r represents the Laplace operator in polar coordinates given by,

$$\Delta_r u(r,\theta) = \frac{1}{r}\frac{\partial}{\partial r}\left(r\frac{\partial u}{\partial r}\right) + \frac{1}{r^2}\frac{\partial^2 u}{\partial \theta^2}, \tag{2}$$

which is obtained using the transformations $x = r\cos\theta$ and $y = r\sin\theta$. At a macroscopic level, the combined random walks of numerous microscopic particles are well approximated by Fickian diffusion and cross-diffusion.

Remark. Note that, for the cross-diffusive system to be well-posed, the main diffusion parameter d and cross-diffusion parameters d_u and d_v must exist in a way that $d - d_u d_v > 0$. This is the so-called normally elliptic condition on the diffusion parameters d, d_u and d_v which requires that the diffusion tensor matrix is positive definite and that entails that $d - d_u\, d_v > 0$. This regularity condition ensures the well-posedness of the system of partial differential equations [45]. This elliptic condition also ensures the global existence and uniqueness of solutions for the full nonlinear system, provided the reaction-kinetics given by $f(u,v)$ and $g(u,v)$ are Lipschitz continuous or that they satisfy maximum principles (see [45] Chapter 14). For details, on classical global existence and uniqueness of solutions of reaction–diffusion in the absence of cross-diffusion, see the work of [45], Chapter 14. The proof of the global existence and uniqueness of the solutions for system (1) in the presence of linear cross-diffusion should follow similar arguments, however, this is not a trivial calculation.

It must be noted that if the condition on the positivity of the determinant of the diffusion matrix is satisfied, then the boundary conditions can be written as,

$$\frac{\partial u}{\partial r} = \frac{\partial v}{\partial r} = 0. \tag{3}$$

System (1) is posed on a circular domain defined as $\Omega = \{(x,y) \in \mathbb{R}^2 : x^2 + y^2 < \rho^2\}$ and its boundary is given by $\partial\Omega = \{(x,y) \in \mathbb{R}^2 : x^2 + y^2 = \rho^2\}$. The parameter d in System (1) denotes the ratio of the diffusion coefficients as $d = \dfrac{D_v}{D_u}$, while $d_u = \dfrac{D_{uv}}{D_u}$ and $d_v = \dfrac{D_{vu}}{D_u}$ denote the ratio between the cross-diffusion coefficients and the diffusion coefficient of the u component. Here, D_u and D_v represent dimensional diffusion coefficients of the components u and v respectively, and D_{uv} and D_{vu} represent dimensional cross-diffusion coefficients of the components u and v respectively. Details on the nondimensionalization process of System (1) are presented in [11].

In System (1) the functions $f(u,v) = \alpha - u + u^2 v$ and $g(u,v) = \beta - u^2 v$ denote the nonlinear activator-depleted reaction kinetics where α and β are non-dimensional positive constants [1,3,14].

It must be noted that the eigenvalues of the Kronecker product of the diffusion matrix and the Laplacian (like here, we have $D \otimes \Delta$ — with D the diffusion matrix and Δ the Laplacian) are given by all combinations of products of the eigenvalues of the diffusion matrix and the Laplacian, that is, if μ is an eigenvalue of the Laplacian, and if λ is an eigenvalue of the diffusion matrix, then $\mu\lambda$ is an eigenvalue of the Kronecker product of the diffusion matrix and the Laplacian.

2. Stability analysis in the presence of cross-diffusion on disc shape domain

The activator-depleted model given by System (1) admits a constant uniform steady state unique solution $(u_s, v_s) = (\alpha + \beta, \frac{\beta}{(\alpha+\beta)^2})$ [1,11,12]. The uniform steady-state is a unique stationary point where the reaction kinetics satisfy $f(u_s, v_s) = g(u_s, v_s) = 0$, as well as the zero-flux boundary condition of System (1). Stability analysis is performed using the linear stability theory to locally perturb System (1), and thus we proceed by investigating the local evolution of the dynamics of the perturbed variables, namely, $(u,v) = (u_s + \epsilon\bar{u}, v_s + \epsilon\bar{v})$, with $0 < \epsilon \ll 1$, that is, in the neighbourhood of the uniform steady state. Employing asymptotic expansions and the Taylor expansion, ignoring $O(\epsilon^2)$ and any higher order terms on the functions of the two variables, leads to the derivation of a linearized reaction–diffusion system (1), with linear cross-diffusion, which we write in matrix–vector form as

$$\bar{\mathbf{w}}_t = \mathbf{D}\Delta_r \bar{\mathbf{w}} + \gamma \mathbf{J_F} \bar{\mathbf{w}}. \tag{4}$$

Here, the solution vector $\bar{\mathbf{w}}$, diffusion coefficient matrix $\mathbf{D}$, reaction kinetics vector $\mathbf{F}$, and the Jacobian matrix $\mathbf{J_F}$ are expressed as

$$\bar{\mathbf{w}} = \begin{bmatrix} \bar{u} \\ \bar{v} \end{bmatrix}, \mathbf{D} = \begin{bmatrix} 1 & d_v \\ d_u & d \end{bmatrix}, \mathbf{F}(u,v) = \begin{bmatrix} f(u_s, v_s) \\ g(u_s, v_s) \end{bmatrix}, \mathbf{J_F} = \begin{bmatrix} f_u(u_s, v_s) & f_v(u_s, v_s) \\ g_u(u_s, v_s) & g_v(u_s, v_s) \end{bmatrix}. \tag{5}$$

For the interested reader on linear stability analysis, we refer the reader to works by Turing [7], Murray [1] and Madzvamuse [5].

We proceed with the linearization procedure by finding the eigenfunctions of Laplace operator satisfying the homogeneous Neumann boundary conditions. Such eigenfunctions for the Laplace operator are obtained by solving the following eigenvalue problem,

$$\begin{cases} \Delta_r w = -k^2 w, & k \in \mathbb{R} \\ \dfrac{\partial w}{\partial r}\Big|_{r=\rho} = 0 & \rho \in \mathbb{R}_+ \setminus \{0\}, \end{cases} \tag{6}$$

where Δ_r represents the Laplace operator on a disc shape domain presented in (2). The method of separation of variables is applied to the eigenvalue problem (6), thereby enabling us to find a solution as $w(r,\theta) = R(r)\Theta(\theta)$. The following theorem indicates the solution of the eigenvalue problem (6).

Theorem 1. *Let $w(r,\theta)$ satisfy the eigenvalue problem (6) under the homogeneous Neumann boundary conditions and n be the order of Bessel's function in $\mathbb{R} \setminus \frac{1}{2}\mathbb{Z}$. Then, for a fixed pair (n,m), with m any positive integer, there exists an infinite set of eigenfunctions of the Laplace operator in the form of [16]*

$$w_{n,m}(r,\theta) = [R^1_{n,m}(r) + R^2_{n,m}(r)]\Theta_n(\theta) \tag{7}$$

where $R^1_{n,m}(r)$ and $R^2_{n,m}(r)$ represent the Bessel functions of first kind given as

$$\begin{cases} R^1_{n,m}(r) = \displaystyle\sum_{j=0}^{\infty} \frac{(-1)^j C_0 (r\, k_{n,m})^{2j+n}}{4^j j!(n+j)(n+j-1)\cdots(n+1)} \\ R^2_{n,m}(r) = \displaystyle\sum_{j=0}^{\infty} \frac{(-1)^j C_0 (r\, k_{n,m} r)^{2j-n}}{4^j j!(-n+j)(-n+j-1)\cdots(-n+1)} \end{cases} \tag{8}$$

for $j = 2m$. Here, C_0 is the first coefficient of the Bessel series. $\Theta_n(\theta)$ is expressed as

$$\Theta_n(\theta) = e^{(n\theta i)}. \tag{9}$$

In the above, $k^2_{n,m}$ represents the eigenmodes which are defined by

$$k^2_{n,m} = \frac{4(2m+1)(n+2m+1)(n+4m)}{\rho^2(n+4m+2)}. \tag{10}$$

Proof. The solution procedure of the eigenvalue problem requires the applications of the same steps as presented in [16]. □

Now we can write the solution of the linearized system (1), following the above standard method of separation of variables for the solution of the eigenvalue problem (6) on a disc domain in closed form expansion of the basis of the eigenfunctions defined by,

$$u(r,\theta,t) = \sum_{m=0}^{\infty} U_{n,m} e^{\lambda_{(n,m)} t} R_{n,m}(r)\Theta_n(\theta) \tag{11}$$

$$v(r,\theta,t) = \sum_{m=0}^{\infty} V_{n,m} e^{\lambda_{(n,m)} t} R_{n,m}(r)\Theta_n(\theta), \tag{12}$$

where $U_{n,m}$ and $V_{n,m}$ represent coefficients corresponding to the eigenfunctions in the eigen-expansion of the series solution to (6). Substituting the solutions (11) and (12) into System (1) gives the fully linearized form of (1) as a system of ordinary differential equations (ODEs) given by

$$\frac{\partial}{\partial t}\begin{bmatrix} \bar{u} \\ \bar{v} \end{bmatrix} = \begin{bmatrix} -k^2_{n,m} + \gamma f_u(u_s, v_s) & -d_v k^2_{n,m} + \gamma f_v(u_s, v_s) \\ -d_u k^2_{n,m} + \gamma g_u(u_s, v_s) & -d k^2_{n,m} + \gamma g_v(u_s, v_s) \end{bmatrix} \begin{bmatrix} \bar{u} \\ \bar{v} \end{bmatrix}. \tag{13}$$

Since we know explicitly the uniform steady state, $(u_s, v_s) = (\alpha+\beta, \frac{\beta}{(\alpha+\beta)^2})$, the individual entries of the Jacobian matrix in System (13) can be computed explicitly. We exploit this to find the partial derivatives of the reaction kinetics $f(u,v)$ and $g(u,v)$ evaluated at the uniform steady state solutions (u_s, v_s), explicitly in terms of the system parameters. Therefore, we write the following two-component dynamical system (13) in the form of a two-component discrete eigenvalue problem as

$$\begin{bmatrix} \gamma\frac{\beta-\alpha}{\alpha+\beta} - k^2_{n,m} & \gamma(\beta+\alpha^2) - d_v k^2_{n,m} \\ -\gamma\frac{2\beta}{\alpha+\beta} - d_u k^2_{n,m} & -\gamma(\beta+\alpha^2) - d k^2_{n,m} \end{bmatrix} \begin{bmatrix} \bar{u} \\ \bar{v} \end{bmatrix} = \lambda \begin{bmatrix} \bar{u} \\ \bar{v} \end{bmatrix}. \tag{14}$$

To proceed, we find the corresponding characteristic polynomial for (14) in λ. The characteristic polynomial satisfying the System (14) in λ can be written as

$$\begin{vmatrix} \gamma\frac{\beta-\alpha}{\alpha+\beta} - k_{n,m}^2 - \lambda & \gamma(\beta+\alpha^2) - d_v k_{n,m}^2 \\ -\gamma\frac{2\beta}{\alpha+\beta} - d_u k_{n,m}^2 & -\gamma(\beta+\alpha^2) - d k_{n,m}^2 - \lambda \end{vmatrix} = 0, \tag{15}$$

which corresponds to a quadratic polynomial in λ. It can be easily shown that the characteristic polynomial can be expressed as

$$\left(\gamma\frac{\beta-\alpha}{\alpha+\beta} - k_{n,m}^2 - \lambda\right)\left(-\gamma(\beta+\alpha^2) - d k_{n,m}^2 - \lambda\right) - \left(\gamma(\beta+\alpha^2) - d_v k_{n,m}^2\right)\left(-\gamma\frac{2\beta}{\alpha+\beta} - d_u k_{n,m}^2\right) = 0. \tag{16}$$

Written more compactly in terms of the trace and the determinant of the stability matrix on the left hand-side of (16), the characteristic polynomial becomes

$$\lambda^2 - \mathcal{T}(\alpha,\beta)\lambda + \mathcal{D}(\alpha,\beta) = 0, \tag{17}$$

where $\mathcal{T}(\alpha,\beta)$ and $\mathcal{D}(\alpha,\beta)$ represent the trace and the determinant of the stability matrix, respectively. Thus, the eigenvalues are obtained as the roots of the quadratic Eq. (17) and are given by

$$\lambda_{1,2} = \frac{\mathcal{T}(\alpha,\beta) \mp \sqrt{\mathcal{T}^2(\alpha,\beta) - 4\mathcal{D}(\alpha,\beta)}}{2}. \tag{18}$$

We compute the $\mathcal{T}(\alpha,\beta)$ and $\mathcal{D}(\alpha,\beta)$ of the matrix given in (14) as follows

$$\mathcal{T}(\alpha,\beta) = \gamma\left(\frac{\beta-\alpha}{\alpha+\beta} - (\beta+\alpha)^2\right) - (d+1)k_{n,m}^2 \tag{19}$$

and

$$\mathcal{D}(\alpha,\beta) = \left(\gamma\frac{\beta-\alpha}{\alpha+\beta} - k_{n,m}^2\right)\left(-\gamma(\beta+\alpha)^2 - d k_{n,m}^2\right) - \left(\gamma(\beta+\alpha)^2 - d_v k_{n,m}^2\right)\left(-\gamma(\frac{-2\beta}{\alpha+\beta}) - d_u k_{n,m}^2\right). \tag{20}$$

The roots of the characteristic equation include a parameter representing the domain size of the disc, given by ρ as well as all other model parameters. Now, the relationship between the domain-size controlling parameter ρ and the rest of the model parameters is explored through the analysis of $\mathcal{T}(\alpha,\beta)$ and $\mathcal{D}(\alpha,\beta)$. Note that the cross-diffusion parameters d_u and d_v appear only in determinant of the stability matrix $\mathcal{D}(\alpha,\beta)$, whereas $\mathcal{T}(\alpha,\beta)$ is independent of the cross-diffusion parameters d_u and d_v. In the following section, we present conditions for the dynamics of cross-diffusive reaction–diffusion system to exhibit both spatial (time-independent) and spatiotemporal (time-dependent) pattern formation on disc-shape domains.

2.1. Domain-dependent analysis for spatiotemporal pattern formation on the disc-shape domain

For stability, the eigenvalues of the matrix in Eq. (13) need to have a non-positive real part. Assuming $\alpha,\beta \in \mathbb{R}_0^+$, linear stability is warranted if $\mathcal{T}(\alpha,\beta) \le 0$ and $\mathcal{D}(\alpha,\beta) \ge 0$. Then two possibilities occur: If $0 \le \mathcal{D}(\alpha,\beta) \le \frac{\mathcal{T}^2(\alpha,\beta)}{4}$, then the eigenvalues are all negative (hence real-valued), whereas if $\frac{\mathcal{T}^2(\alpha,\beta)}{4} < \mathcal{D}(\alpha,\beta)$, then the eigenvalues are non-real. In the sequence below, we detail the analysis of the stability of Eq. (13).

To derive the conditions on the domain-size, we analyse the characteristic polynomial (17), when the roots of (17) consists of a complex-conjugate pair. We first consider the partition of the parameter plane $(\alpha,\beta) \in \mathbb{R}_+^2$ by the following curve

$$\mathcal{T}^2(\alpha,\beta) - 4\mathcal{D}(\alpha,\beta) = 0. \tag{21}$$

Eq. (21) is a partitioning curve which admits on one side of the curve the regions when $\lambda_{1,2} \in \mathbb{R}$ and on the other side, corresponds to $\lambda_{1,2} \in \mathbb{C}\backslash\mathbb{R}$. The eigenvalues $\lambda_{1,2}$ are a complex conjugate pair if $(\alpha,\beta) \in \mathbb{R}_+^2$ satisfy the following inequality

$$\mathcal{T}^2(\alpha,\beta) - 4\mathcal{D}(\alpha,\beta) < 0. \tag{22}$$

Given that the inequality (22) is satisfied, one must admit $\mathcal{D}(\alpha,\beta) > 0$. We note that the trace of the stability matrix is independent of cross-diffusion terms d_u and d_v and therefore the domain-dependent conditions proven in [16] without cross-diffusion remain unchanged. Restricting the analysis to the trace of the stability matrix in the presence of linear cross diffusion yields the same results as those obtained in the absence of cross-diffusion. It is only through the analysis of the determinant of the stability matrix that the effects of linear cross-diffusion can be studied. In particular, we will explore the positivity of $\mathcal{D}(\alpha,\beta)$. Before we proceed, we first recall the statements of Theorems 2 and 3 in [16] in the spirit of our model posed on a disc-shaped domain, in the absence of cross-diffusion. We note that the following two theorems are established based on the analysis of the trace of the stability matrix (13), and the trace $\mathcal{T}$ includes only the main diffusion coefficient d. Later on, we will state extensions of such theorems when cross-diffusion terms are taken into account, which require the analysis of $\mathcal{D}$ of the stability matrix since cross-diffusion terms d_u and d_v appear explicitly in $\mathcal{D}$.

Theorem 2 (*Condition for Hopf/Transcritical Bifurcation*). *Let u and v satisfy the cross-diffusive reaction–diffusion system (1) with positive parameters $\alpha > 0$, $\beta > 0$, $d > 0$, and $\gamma > 0$ on a disc-shape domain with radius ρ. For System (1) to exhibit Hopf and/or transcritical bifurcations, the domain-size controlling parameter ρ of the disc shape must be large enough satisfying*

$$\rho^2 \geq \frac{4(d+1)(2m+1)(n+2m+1)(n+4m)}{\gamma(n+4m+2)}, \tag{23}$$

where $n \in \mathbb{R} \setminus \frac{1}{2}\mathbb{Z}$ is the associated order of the Bessel's equation and m is any positive integer.

Proof. The proof of this theorem is accomplished through the positivity of the trace $\mathcal{T}(\alpha, \beta)$ of the stability matrix given by (13). Note that, the trace $\mathcal{T}(\alpha, \beta)$ of the stability of matrix (13) is independent of cross-diffusive coefficients, it includes only the main diffusion coefficient d. Therefore we conclude that, the requirement for the system to exhibit Hopf/transcritical bifurcations stays the same as those of the case without cross-diffusion, yet producing the condition on domain size parameter ρ in terms of the main diffusion coefficient d, only. The proof of this theorem for the case of no cross-diffusion is presented in [16]. □

Theorem 3 (*Turing Diffusion-Driven Instability*). *Let u and v satisfy the cross-diffusive reaction–diffusion system (1) with real positive parameters $\alpha > 0$, $\beta > 0$, $d > 0$, and $\gamma > 0$ on the disc shape domain $\Omega \in \mathbb{R}^2$ with radius ρ. If the domain-size controlling parameter ρ satisfies the condition*

$$\rho^2 < \frac{4(d+1)(2m+1)(n+2m+1)(n+4m)}{\gamma(n+4m+2)}, \tag{24}$$

then the instability of the cross-diffusive system (1) is restricted to Turing type only, which means under this condition temporal periodicity in the dynamics is forbidden. In (24), $n \in \mathbb{R} \setminus \frac{1}{2}\mathbb{Z}$ is the associated order of the Bessel's equation and m is any positive integer.

Proof. The proof of this theorem is acquired through exploring the real part of the eigenvalues $\lambda_{1,2}$ when the discriminant $\mathcal{T}^2 - 4D$ of the characteristic polynomial is negative. The surface $\mathcal{T}(\alpha, \beta)$ is analysed within the range of the admissible unstable parameter spaces $(\alpha, \beta) \subset \mathbb{R}^2$ using the monotonicity conditions and Hessian matrix which leads to condition (24). We note that the current analysis is based on the fact that the trace $\mathcal{T}(\alpha, \beta)$ of the stability matrix (13) is independent of d_u and d_v. Therefore, we conclude that the requirement of Theorem 3 stays same in the case without cross-diffusion. The proof of this theorem for the case of no cross-diffusion is presented in [16]. □

Remark. Note that Theorem 2 is the necessary condition for the system to exhibit Hopf/transcritical type of bifurcation, however it does not exclude the existence of the Turing type instability. However, Theorem 3 forbids the existence of temporal periodicity. To appreciate the contributions of cross-diffusion to the classical reaction–diffusion theory, we analyse the conditions when the cross-diffusion coefficients d_u and d_v are taken into account. This entails studying when the determinant of the stability matrix $\mathcal{D}(\alpha, \beta)$ is positive. We proceed with the expansion of the determinant of the stability matrix (13) and write it in the form of a product of a strictly positive quantity $\frac{1}{\alpha+\beta}$ with a cubic polynomial in β as follows

$$\mathcal{D}(\alpha, \beta) = p_0 + p_1\beta + p_2\beta^2 + p_3\beta^3, \tag{25}$$

where

$$p_0 = \frac{1}{\alpha+\beta}\kappa_0(\alpha), \quad p_1 = \frac{1}{\alpha+\beta}\kappa_1(\alpha), \quad p_2 = \frac{1}{\alpha+\beta}\kappa_2(\alpha), \quad \text{and} \quad p_3 = \frac{1}{\alpha+\beta}\kappa_3(\alpha).$$

Here, the κ_i's ($i = 0, 1, 2, 3$) are expanded in terms of all the remaining parameters of the system and these can be shown to be given by

$$\kappa_0(\alpha) = \alpha^3\gamma^2 + \alpha^3\gamma k_{n,m}^2 + \alpha d k_{n,m}^4 - \alpha d_u d_v k_{n,m}^4 + \alpha d\gamma k_{n,m}^2 + \alpha^3 d_u \gamma k_{n,m}^2, \tag{26}$$

$$\kappa_1(\alpha) = d k^4 - d_u d_v k_{n,m}^4 - d\gamma k_{n,m}^2 + 3\alpha^2\gamma^2 + 3\alpha^2\gamma k_{n,m}^2 + 3\alpha^2 d_u \gamma k_{n,m}^2 - 2 d_v \gamma k_{n,m}^2, \tag{27}$$

$$\kappa_2(\alpha) = 3\alpha\gamma(k_{n,m}^2(d_u + 1) + \gamma), \tag{28}$$

$$\kappa_3(\alpha) = \gamma k_{n,m}^2 + \gamma^2 + d_u\gamma k_{n,m}^2 = \gamma(k_{n,m}^2(d_u + 1) + \gamma). \tag{29}$$

Note that since $\alpha, \beta \in \mathbb{R}_0^+$, therefore, we assert that $D(\alpha, \beta) > 0$ requires the positivity of the cubic polynomial in β given in (25). We start by normalizing the polynomial such that the coefficient of β^3 is one, which implies that we can write

$$\beta^3 + \frac{\kappa_2(\alpha)}{\kappa_3(\alpha)}\beta^2 + \frac{\kappa_1(\alpha)}{\kappa_3(\alpha)}\beta + \frac{\kappa_0(\alpha)}{\kappa_3(\alpha)} > 0. \tag{30}$$

The domain-size controlling parameter ρ, which is the radius of disc, is now used as a parameter of the coefficients of (30). In light of the following theorem given in [46], we aim to obtain the conditions required for (30) to hold, in terms of ρ, d, d_u, d_v, γ, and the spectrum of the Laplace operator.

Theorem 4 (*Conditions on Positivity for a Cubic Polynomial*). *Let $\mathcal{D}(\beta) = \beta^3 + a\beta^2 + b\beta + c$ be defined as non-degenerate cubic polynomial. For the positivity of $\mathcal{D}(\beta)$, the following conditions must be satisfied;*

$$(i)\ c > 0, \quad (ii)\ a, b \geq 0, \quad \text{and} \quad (iii)\ \Delta(\beta) = a^2b^2 + 18abc - 27c^2 - 4a^3c - 4b^3 \leq 0$$

where $\Delta(\beta)$ represents the discriminant of $\mathcal{D}(\beta)$.

Proof. The proof can be found in [47] . □

The three conditions on a, b, and c in Theorem 4 are represented in terms of the system parameters as follows

$$a = \frac{\kappa_2(\alpha)}{\kappa_3(\alpha)} = \frac{3\alpha\gamma^2 + 3\alpha\gamma k_{n,m}^2 + 3\alpha d_u\gamma k_{n,m}^2}{\gamma k_{n,m}^2 + \gamma^2 + d_u\gamma k_{n,m}^2} \geq 0, \tag{31}$$

$$b = \frac{\kappa_1(\alpha)}{\kappa_3(\alpha)} = \frac{(d - d_u d_v)k_{n,m}^4 - (d\gamma - 3\alpha^2\gamma - 3\alpha^2 d_u\gamma - 2d_v\gamma)k_{n,m}^2}{\gamma k_{n,m}^2 + \gamma^2 + d_u\gamma k_{n,m}^2} + \frac{3\alpha^2\gamma^2}{\gamma k_{n,m}^2 + \gamma^2 + d_u\gamma k_{n,m}^2} \geq 0, \tag{32}$$

and

$$c = \frac{\kappa_0(\alpha)}{\kappa_3(\alpha)} = \frac{(d - d_u d_v)\alpha k_{n,m}^4 + (\alpha^3\gamma + \alpha d\gamma + \alpha^3 d_u\gamma)k_{n,m}^2 + \alpha^3\gamma^2}{\gamma k_{n,m}^2 + \gamma^2 + d_u\gamma k_{n,m}^2} > 0. \tag{33}$$

Proposition 1. *Let the cubic polynomial $\mathcal{D}(\beta)$ in Theorem 4 be described as*

$$\mathcal{D}(\beta) = h(\beta)\beta + c, \tag{34}$$

where $h(\beta) = \beta^2 + a\beta + b$, with a, b, c given by (31)–(33) and $\beta \geq 0$. The non-negativity of the quadratic polynomial $h(\beta)$ must satisfy that either $a \geq 0$, $b \geq 0$, or $b > 0$, $4b \geq a^2$. This means that the cubic polynomial $\mathcal{D}(\beta)$ is strictly positive for all $\beta \geq 0$ and $c > 0$ satisfying the above conditions.

Proof. The proof of this Proposition is presented in [46,47]. □

The influence of the domain size controlling parameter ρ^2 on system parameters including cross-diffusion coefficients is explored by the following theorem.

Theorem 5 (*Condition on ρ for Spatiotemporal Pattern Formation of Cross-Diffusive System*). *For the reaction–diffusion system (1) with linear cross-diffusion to exhibit spatio-temporal pattern formation, the domain size controlling parameter ρ must satisfy,*

$$\rho^2 > \frac{4(d - d_u d_v)(2m + 1)(n + 2m + 1)(n + 4\ m)}{(7d + 8d_v)(n + 4m + 2)\gamma}. \tag{35}$$

Proof. Manipulating the inequality (31) through algebraic operations yields a straightforward condition as $3\alpha \geq 0$. This requirement arises from the fact that $(\alpha, \beta) \in \mathbb{R}_+^2$ in System (1). By employing the second condition outlined in Proposition 1 to ensure the positivity of $D(\beta)$, we are now able to express the following conditions,

$$\begin{cases} 3\alpha^2 + \dfrac{(d - d_u d_v)k_{n,m}^4 - (d + 2d_v)\gamma k_{n,m}^2}{(1 + d_u)\gamma k_{n,m}^2 + \gamma^2} \geq \dfrac{9\alpha^2}{4}, \\ \alpha^2 + \dfrac{(d - d_u d_v)k_{n,m}^4 + d\gamma k_{n,m}^2}{(1 + d_u)\gamma k_{n,m}^2 + \gamma^2} > 0. \end{cases} \tag{36}$$

The conditions of (36) are simplified as follows

$$\frac{4(d - d_u d_v)k_{n,m}^4 - 4(d + 2d_v)\gamma k_{n,m}^2}{(1 + d_u)\gamma k_{n,m}^2 + \gamma^2} \geq -3\alpha^2, \tag{37}$$

and

$$\frac{3(d - d_u d_v)k_{n,m}^4 + 3d\gamma k_{n,m}^2}{(1 + d_u)\gamma k_{n,m}^2 + \gamma^2} > -3\alpha^2. \tag{38}$$

We proceed to analyse a special case of (37) given by the equal sign combined with inequality (38). Hence, we obtain the following system,

$$\begin{cases} \dfrac{4(d - d_u d_v)k_{n,m}^4 - 4(d + 2d_v)\gamma k_{n,m}^2}{(1 + d_u)\gamma k_{n,m}^2 + \gamma^2} = -3\alpha^2, \\ \dfrac{3(d - d_u d_v)k_{n,m}^4 + 3d\gamma k_{n,m}^2}{(1 + d_u)\gamma k_{n,m}^2 + \gamma^2} > -3\alpha^2. \end{cases} \tag{39}$$

Substituting $-3\alpha^2$ from the second inequality into the right-hand term of the first equality leads to the following inequality

$$\frac{3(d-d_u d_v)k_{n,m}^4+3d\gamma k_{n,m}^2}{(1+d_u)\gamma k_{n,m}^2+\gamma^2} > \frac{4(d-d_u d_v)k_{n,m}^4-4(d+2d_v)\gamma k_{n,m}^2}{(1+d_u)\gamma k_{n,m}^2+\gamma^2}. \tag{40}$$

To proceed, we solve (40) for $k_{n,m}^2$ to obtain a sufficient condition, on the radius of the disc, ρ, that will establish the positivity of the cubic polynomial (30), thereby ensuring the positivity of the determinant of the stability matrix given by (25). For the derivation of the desired condition, the sign of the denominator of both sides of (40) is exploited, which requires the analysis to independently investigate the case when the denominator on both sides of (40) is either positive or negative. Such requirement enforces two independent cases to explore, namely $d_u > -1$ or $d_u < -1$, subject to $d - d_u d_v > 0$. Hence, the current analysis admits the concept of cross-diffusion where one of the species can either be negative or positive.

However, the determinant of the diffusion matrix must be positive to guarantee the regularity of the partial differential system. We exploit the experimental investigation presented in [9] and results therein, where both negative and positive cross-diffusion, giving rise to Turing type behaviour in the dynamics. Such experimental findings create the platform to explore the cross-diffusive parameter d_u across the full spectrum of the real line in particular, both for the choice of negative and positive real values. Therefore, exploiting such observations we consider $d_u > -1$, which corresponds to the positivity of the denominator of both sides of (40). As a result, we write

$$3(d-d_u d_v)k_{n,m}^2+3d\gamma > 4(d-d_u d_v)k_{n,m}^2-4(d+2d_v)\gamma \tag{41}$$

or

$$3d\gamma+4(d+2d_v)\gamma > (d-d_u d_v)k_{n,m}^2. \tag{42}$$

Re-arranging inequality (42) results in

$$k_{n,m}^2 < \frac{(7d+8d_v)\gamma}{d-d_u d_v}. \tag{43}$$

Substitution of $k_{n,m}^2 = \dfrac{4(2m+1)(n+2m+1)(n+4\ m)}{\rho^2(n+4m+2)}$ into condition (43) allows us to write the condition on the disc radius ρ as,

$$\frac{4(2m+1)(n+2m+1)(n+4\ m)}{\rho^2(n+4m+2)} < \frac{(7d+8d_v)\gamma}{d-d_u d_v}. \tag{44}$$

Inequality (44) is re-arranged to yield the desired condition,

$$\rho^2 > \frac{4(d-d_u d_v)(2m+1)(n+2m+1)(n+4\ m)}{(7d+8d_v)(n+4m+2)\gamma}, \tag{45}$$

which completes the proof. □

Remark. Note that, for the cross-diffusive system to be well-posed, the main diffusion parameter d and cross-diffusion parameters d_u and d_v must exist in a way that $d - d_u d_v > 0$. The above analysis assumes this condition holds as part of the cross-diffusive driven instability condition, i.e. the determinant of the diffusion matrix given in Eq. (5) must be positive. The proof of this condition is shown in [11].

3. Numerical classification of the unstable regions

In this section, we plot the parameter spaces characterized by positive α and β values to validate our theoretical results by varying the system parameters d, d_u, d_v and γ. The partition curve which separates the regions defining real and complex roots must satisfy

$$\mathcal{T}^2 - 4D = 0, \tag{46}$$

which indicates which regions are characterized by repeated real, real and different and complex eigenvalues. The nature of the eigenvalues are determined by the sign of discriminant $\mathcal{T}^2 - 4D$. We proceed to define $\mathcal{T}^2 - 4D$ implicitly as a 6th order polynomial in β using system parameters d, d_u, d_v, γ and α in (46) as

$$\Psi(\alpha,\beta) = \mathcal{P}_0(\alpha)+\mathcal{P}_1(\alpha)\beta+\mathcal{P}_2(\alpha)\beta^2+\mathcal{P}_3(\alpha)\beta^3+\mathcal{P}_4(\alpha)\beta^4+\mathcal{P}_5(\alpha)\beta^5+\mathcal{P}_6(\alpha)\beta^6, \tag{47}$$

where the coefficients $\mathcal{P}_i$'s are expanded as

$$\begin{aligned}
\mathcal{P}_0 &= \gamma^2\alpha^6+2\gamma\alpha^4(-\gamma+(d-2d_u-1)k_{n,m}^2)+\gamma^2\alpha^2-2\alpha^2(d-1)\gamma k_{n,m}^2+\alpha^2(d+4d_u d_v-2d+1)k_{n,m}^4,\\
\mathcal{P}_1 &= 6\gamma^2\alpha^5-12\gamma^2\alpha^3+8\gamma\alpha^3(d-2d_u-1)k_{n,m}^2-\gamma^2-4d_v k_{n,m}^2+(d^2+4d_u d_v-2d+1)k_{n,m}^4,\\
\mathcal{P}_2 &= 15\gamma^2\alpha^4-24\gamma\alpha^2+12\gamma\alpha^2(d-2d_u-1)k_{n,m}^2+\gamma^2+2(d+4d_v-1)k_{n,m}^2+\gamma+(d^2+4d_u d_v-2d+1)k_{n,m}^4,\\
\mathcal{P}_3 &= 5\alpha^3\gamma-5\gamma^2\alpha+8\gamma\alpha(d-2d_u-1)k_{n,m}^2,\\
\mathcal{P}_4 &= 15\gamma^2\alpha^2-6\gamma^2+2\gamma(d-2d_u-1)k_{n,m}^2,\\
\mathcal{P}_5 &= 6\alpha\gamma^2, \quad \text{and} \quad \mathcal{P}_6 = \gamma^2.
\end{aligned}$$

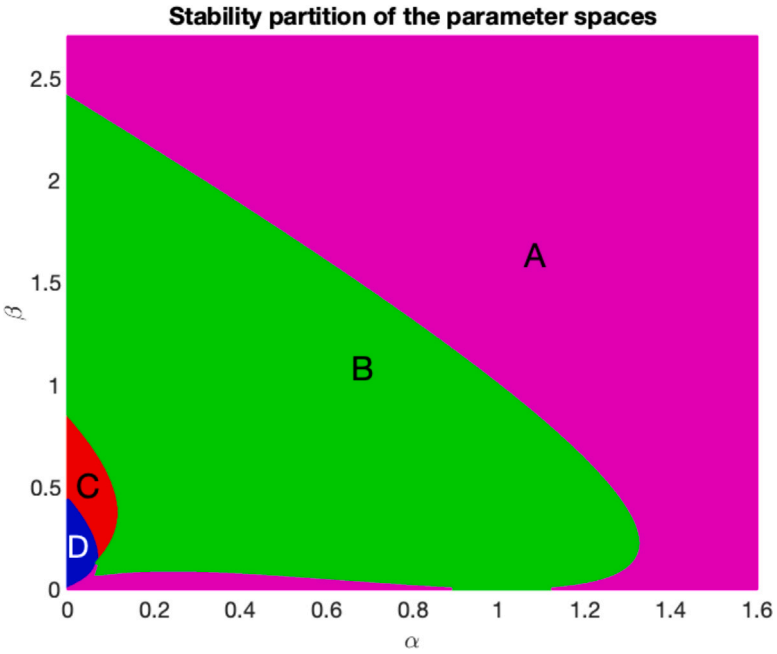

Fig. 1. Classification of the parameter spaces for the reaction–diffusion system with linear cross-diffusion for model parameters $d = 2$, $d_u = d_v = 0.1$, $\gamma = 10$. A: A region with real-distinct negative eigenvalues, B: A region with complex-conjugate eigenvalues with negative real part, C: A region with complex-conjugate eigenvalues with positive real part, D: A region with real-distinct eigenvalues with at least one positive eigenvalue. (For interpretation of the references to colour in this figure legend, the reader is referred to the web version of this article.)

By fixing all model parameters except β, Eq. (47) determines the boundary between stable and unstable regions. We have adopted a similar algorithm and approach presented in [15] where the parameter classification is performed for the classical RDS, in the absence of cross-diffusion. Using the conditions presented in Section 2, the full classification of the stable and unstable regions on (α, β) plane is illustrated in Fig. 1. Each segment presents the regions of stable and unstable regions with real and complex eigenvalues.

The regions where the real part of the eigenvalues (whether purely real or complex) is positive correspond to unstable regions, by which the uniform steady state solution (u_s, v_s) is asymptotically unstable. Stable regions for the uniform steady state solution are those where the real part of the eigenvalues is negative. Regions that allow Turing pattern formation to emerge are those associated with the instability of the uniform steady state solution when the eigenvalues are real or are a complex conjugate pair.

The region corresponding to the real distinct eigenvalues is shown in magenta colour in segment A, and the parameters chosen from this region result in the solutions (u_s, v_s) becoming uniformly stable. Similarly, parameters chosen from the segment B in the green region, show that eigenvalues are complex with a negative real part, entailing that the solutions are asymptotically stable. Regions showing unstable spaces presented by the segments C and D, where the uniform steady state solution is unstable, are given by the colours in red and blue, respectively. We observe a Hopf bifurcation in the system dynamics when the parameters are selected from the red region. Parameters chosen from the blue region indicate that eigenvalues are real and distinct with at least one positive root, where we can observe Turing type of patterns. Further investigation of unstable regions are performed by varying system parameters d, d_u, d_v and γ within the α and β plane.

We begin with the plots of unstable spaces, where the system parameters d, d_u, d_v and γ are varied to give rise to spatiotemporal pattern formation, satisfying the conditions of Theorems 2 and 5. Fig. 2(a)–(d) present the regions on the admissible parameter space α and β corresponding to the complex eigenvalues with a positive real part indicating Hopf bifurcation regions, and pure imaginary eigenvalues indicating the transcritical type of bifurcations. In Fig. 2(a), the effect of the self diffusion parameter d is presented, while the rest of the parameters are fixed. Hopf bifurcation regions are represented in segments $A - E$ whereas the transcritical curves are given by $t_1 - t_5$. Hopf bifurcation regions grow when d is decreased, and the limit cycle regions are shifted from t_1 to t_5. Our numerical demonstration include plotting the parameter space for the case when $d = 1$, such a space does not exist if the model system has no cross-diffusion. This region is shown in Fig. 2(a), represented by the largest region, covering each colour segment. On the other hand, an increase in the reaction scaling parameter γ has an opposite effect on the Hopf and transcritical regions compared to an increase in self-diffusion coefficient d. We observe from Fig. 2(b)–(c) that varying the cross-diffusion parameters d_u, and d_v does not change the position of the limit cycle curve, whereas decreasing the linear cross-diffusion coefficients d_u, and d_v results in smaller Hopf bifurcation regions. Parameter values and regions corresponding to Hopf/transcritical type of bifurcations are summarized in Table 1 including each parameter selection in light of the conditions of Theorems 2 and 5.

We proceed with the plots of Turing parameter spaces satisfying the conditions of Theorems 2 and 5 as shown in Fig. 3. We note that when the domain-size ρ satisfies the conditions given in Theorems 2 and 5, then all types of instabilities are allowed. Fig. 3

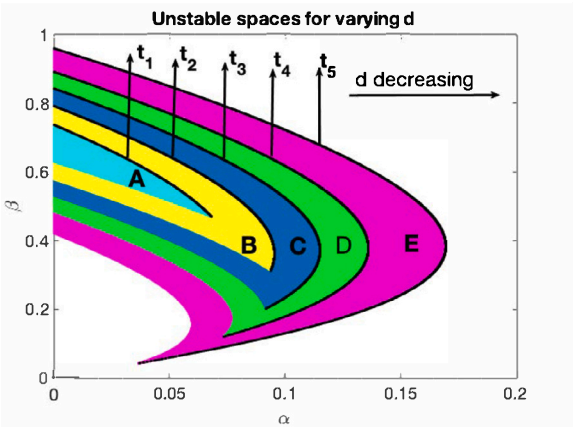

(a)Varying d

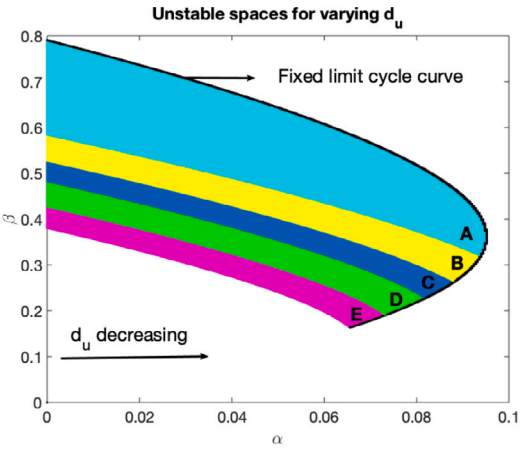

(b)Varying d_u

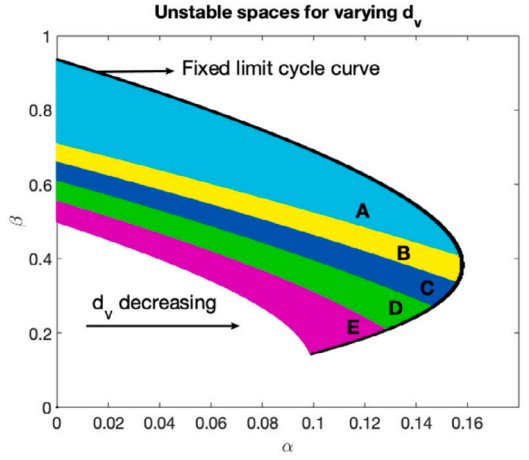

(c) Varying d_v

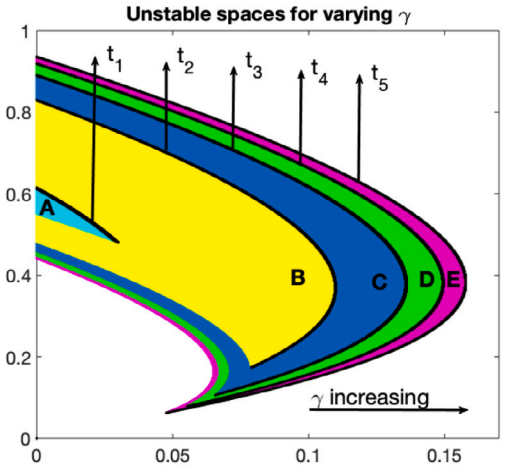

(d) Varying γ

Fig. 2. (a)–(d) Parameter spaces for Hopf bifurcation regions and limit cycle curves with domain-size ρ restricted to satisfy conditions of Theorems 2 and 5 for various system parameters. (For interpretation of the references to colour in this figure legend, the reader is referred to the web version of this article.)

is generated by varying system parameters d, d_u, d_v and γ. These parameters, selected from these segments given by the capital letters, are expected to exhibit spatial periodicity. We observe from Fig. 3(a) that increasing the self diffusion coefficient d results in an increase of the Turing regions. The Turing region for the case $d = 1$ is obtained as is shown by the region A in Fig. 3(a). Again, this region does not exist in the absence of linear cross-diffusion. We observe that an increase in the cross-diffusion coefficient d_u leads to a decrease in Turing spaces, whereas an increase in the cross-diffusion coefficient d_v results in an increase in Turing spaces. Furthermore, an increase in γ gives rise to a decrease in Turing spaces. Details of parameter choice for generation of Turing spaces satisfying the conditions of Theorems 2 and 5 are presented in Table 1.

In Fig. 4, we exhibit Turing spaces that demonstrate the validity of conditions in Theorem 3. These correspond to eigenvalues that are real with at least one of them positive. We observe that variations of system parameters d, d_u, d_v and γ result in similar regions as those shown in Fig. 3. Moreover, the main difference between Figs. 4 and 3 is that, Fig. 4 is generated according to the fact that the condition of Theorem 3 prohibits the existence of Hopf/transcritical type bifurcations and restricts the system to show only Turing type instability. The detailed choice of parameters indicating each segment are presented in Table 2.

4. Numerical simulations with finite element method on disc-shape domain

To validate the theoretical observations presented in Theorems 2, 3, and 5, we present numerical simulations of the model system (1) using the finite element method. For details on the finite element method, we refer the interested readers to [42,48]. The finite element method is characterized by seeking weak solutions which solve a week variational form. This process is then

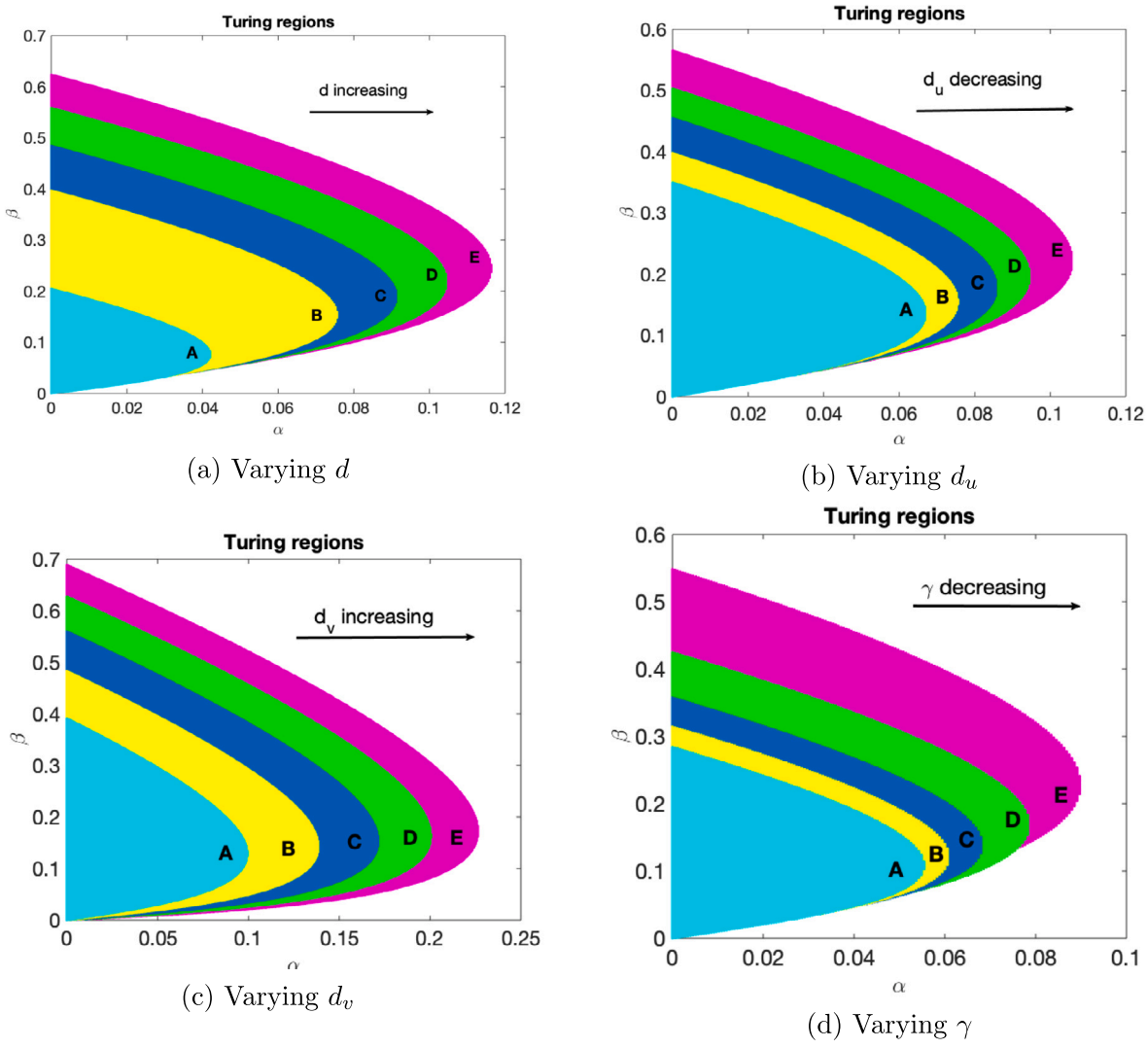

Fig. 3. (a)–(d) Turing spaces with domain-size ρ satisfying conditions of Theorems 2 and 5 for various system parameters.

followed by seeking a weak finite element solution for the space-discretized weak formulation [49,50]. This leads to a system of ordinary differential equations. Domain discretization is one of the key concepts in finite element method. In our work, the finite element mesh for the disc-shape domain is obtained by using an open package domain generator called *Gmsh* [51]. Finally, a time-discretization is carried out to convert the system of ordinary differential equations into a system of nonlinear or linear algebraic equations (depending on the time-stepping scheme employed). We refer the interested to consult the work in [52,53] with regards to time-stepping schemes for reaction–diffusion systems.

We note that the initial conditions are selected to be small random perturbations around the uniform steady-state, presented in [13,15–17] and these are given by,

$$u_0(x,y) = \alpha + \beta + 0.0016\cos(2\pi(x+y)) + 0.01\sum_{n=0}^{8}\cos(n\pi x), \quad \text{and} \quad v_0(x,y) = \frac{\beta}{(\alpha+\beta)^2} + 0.0016\cos(2\pi(x+y)) + 0.01\sum_{n=0}^{8}\cos(n\pi x).$$

Model parameters α and β are selected in light of the parameter spaces generated in Section 3 exhibiting cross-diffusion-driven instability. We keep the size of the radius fixed as $\rho = 1$, and vary the remaining parameters d, d_u, d_v, and γ while ensuring that the conditions of domain-size presented in Section 3 remain valid. In all our numerical simulations, we take 6402 triangular elements, generating 6668 degrees of freedom. Time-discretization is accomplished by using the first-order semi-implicit backward differential formula (1-SBEM) [54] with timestep $\Delta t = 0.001$. For the finite element algorithm, these selected numerical parameters

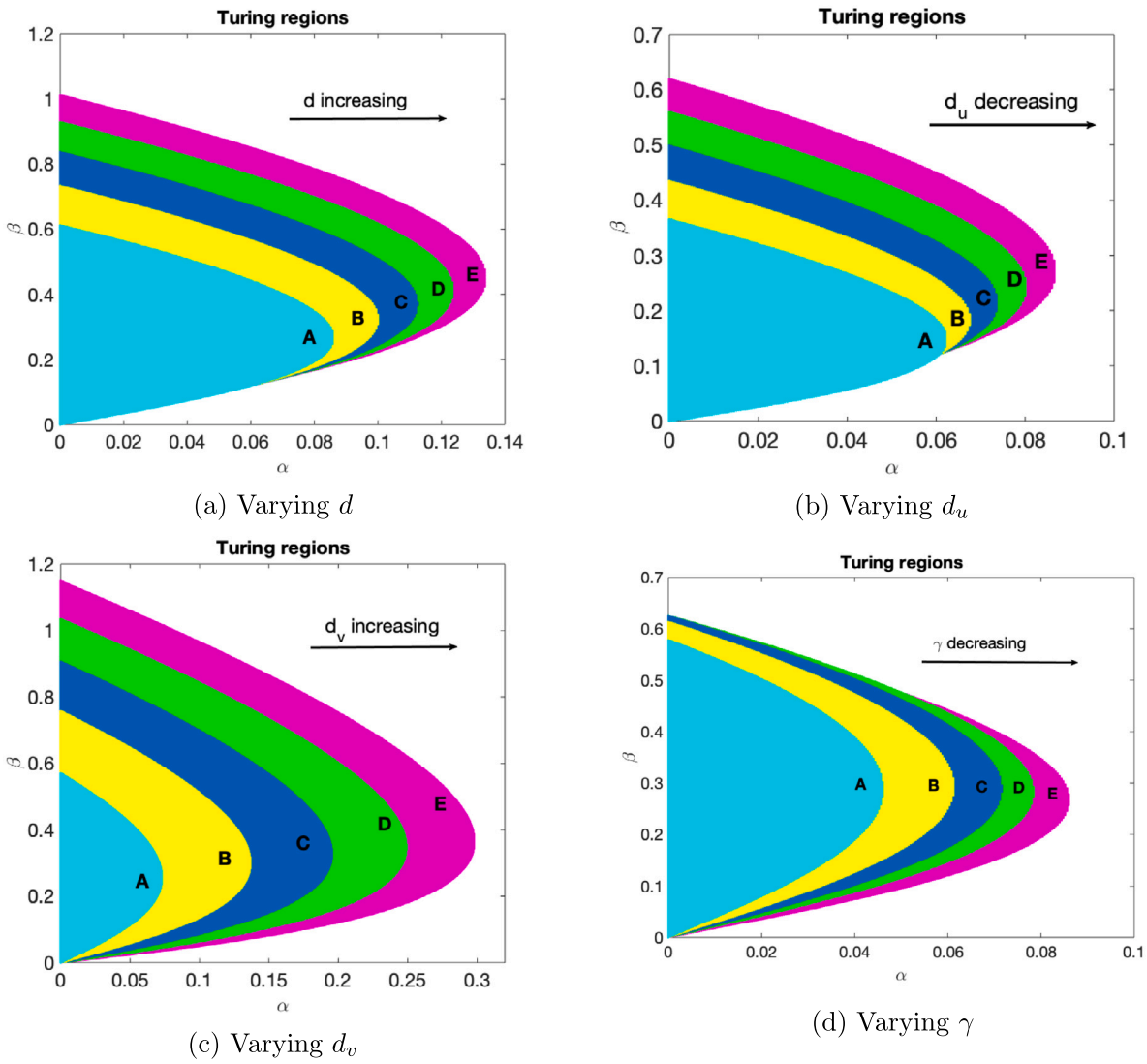

Fig. 4. (a)–(d) Turing spaces with domain-size ρ restricted to satisfy conditions of Theorems 3 and 5 for various system parameters.

satisfy the stability and convergence of the numerical method. Simulations showing the evolution of Turing patterns are presented in Section 4.1, while simulations corresponding to the Hopf and limit cycle behaviour are presented in Section 4.2. Parameter selection information is provided in the captions of each simulations. It must be noted that patterns obtained remained unchanged in all our simulations when the timestep and meshsize are refined (results not shown).

4.1. Spatial pattern formation

Fig. 5 presents the evolution of spatial pattern formation considering the choice of parameters from the Turing region, when the domain-size controlling parameter ρ is subject to the conditions of Theorems 2 and 5, as indicated in Fig. 3. Snapshot series in Fig. 5 show the spatiotemporal evolution of the u profile, starting with the formation of stripe-type patterns which then transform into spatially inhomogeneous spot-patterns. In (h), we plot the L_2 norms of the discrete time derivatives of the u and v-components of the solution to demonstrate the temporal stability behaviour of the solutions as they evolve in time.

The spatiotemporal evolution profile of the u component of the solution for the investigation of the effect of negative cross-diffusion under the conditions of Theorems 2 and 5 is presented in Fig. 6. In particular, the numerical simulation is selected specifically to include the choice of the self-diffusion coefficient as $d = 1$ which does not give rise to pattern formation in the

Table 1
Parameter classification of the instability types when varying d, d_u, d_v, γ to satisfy Theorems 2 and 5.

Figure index	Fig. 2(a)	Fig. 2(a)	Fig. 3(a)
Types of instability	Hopf bifurcation	Transcritical bifurcation	Turing instability
$(\boldsymbol{d}, d_u, d_v, \gamma, \rho)$	$\lambda_{1,2}$		
	$\lambda \in \mathbb{C}, \mathrm{Re}(\lambda_{1,2}) > 0$	$\lambda \in \mathbb{C}, Re(\lambda_{1,2}) = 0$	$0 < \lambda_1 \in \mathbb{R}$ or $0 < \lambda_2 \in \mathbb{R}$
(1,0.1,0.1,10,10)	$A \cup B \cup C \cup D \cup E$	t_5	E
(4,0.1,0.1,10,10)	$A \cup B \cup C \cup D$	t_4	$E \cup D$
(6,0.1,0.1,10,10)	$A \cup B \cup C$	t_3	$E \cup D \cup C$
(8,0.1,0.1,10,10)	$A \cup B$	t_2	$E \cup D \cup C \cup B$
(10,0.1,0.1,10,10)	A	t_1	$E \cup D \cup C \cup B \cup A$
Figure index	Fig. 2(b)	Fig. 2(b)	Fig. 3(b)
Types of instability	Hopf bifurcation	Transcritical bifurcation	Turing instability
$(d, \boldsymbol{d_u}, d_v, \gamma, \rho)$	$\lambda_{1,2}$		
	$\lambda \in \mathbb{C}, \mathrm{Re}(\lambda_{1,2}) > 0$	$\lambda \in \mathbb{C}, Re(\lambda_{1,2}) = 0$	$0 < \lambda_1 \in \mathbb{R}$ or $0 < \lambda_2 \in \mathbb{R}$
(8,−0.5,0.1,10,10)	A	Fixed	$A \cup B \cup C \cup D \cup E$
(8,6,0.1,10,10)	$A \cup B$	Fixed	$A \cup B \cup C \cup D$
(8,13,0.1,10,10)	$A \cup B \cup C$	Fixed	$A \cup B \cup C$
(8,25,0.1,10,10)	$A \cup B \cup C \cup D$	Fixed	$A \cup B$
(8,40,0.1,10,10)	$A \cup B \cup C \cup D \cup E$	Fixed	A
Figure index	Fig. 2(c)	Fig. 2(c)	Fig. 3(c)
Types of instability	Hopf bifurcation	Transcritical bifurcation	Turing instability
$(d, d_u, \boldsymbol{d_v}, \gamma, \rho)$	$\lambda_{1,2}$		
	$\lambda \in \mathbb{C}, \mathrm{Re}(\lambda_{1,2}) > 0$	$\lambda \in \mathbb{C}, Re(\lambda_{1,2}) = 0$	$0 < \lambda_1 \in \mathbb{R}$ or $0 < \lambda_2 \in \mathbb{R}$
(2,0.1,1,10,10)	A	Fixed	A
(2,0.1,2,10,10)	$A \cup B$	Fixed	$A \cup B$
(2,0.1,3,10,10)	$A \cup B \cup C$	Fixed	$A \cup B \cup C$
(2,0.1,4,10,10)	$A \cup B \cup C \cup D$	Fixed	$A \cup B \cup C \cup D$
(2,0.1,5,10,10)	$A \cup B \cup C \cup D \cup E$	Fixed	$A \cup B \cup C \cup D \cup E$
Figure index	Fig. 2(d)	Fig. 2(d)	Fig. 3(d)
Types of instability	Hopf bifurcation	Transcritical bifurcation	Turing instability
$(d, d_u, d_v, \boldsymbol{\gamma}, \rho)$	$\lambda_{1,2}$		
	$\lambda \in \mathbb{C}, \mathrm{Re}(\lambda_{1,2}) > 0$	$\lambda \in \mathbb{C}, Re(\lambda_{1,2}) = 0$	$0 < \lambda_1 \in \mathbb{R}$ or $0 < \lambda_2 \in \mathbb{R}$
(2,0.1,0.1,2,10)	A	t_1	$A \cup B \cup C \cup D \cup E$
(2,0.1,0.1,4,10)	$A \cup B$	t_2	$A \cup B \cup C \cup D$
(2,0.1,0.1,6,10)	$A \cup B \cup C$	t_3	$A \cup B \cup C$
(2,0.1,0.1,8,10)	$A \cup B \cup C \cup D$	t_4	$A \cup B$
(2,0.1,0.1,10,10)	$A \cup B \cup C \cup D \cup E$	t_5	A

Table 2
Parameter classification for Turing instability when varying d, d_u, d_v, γ to satisfy Theorems 3 and 5, forbidding Hopf/transcritical bifurcations.

$(\boldsymbol{d}, d_u, d_v, \gamma, \rho)$/Fig. 4(a)		$(d, \boldsymbol{d_u}, d_v, \gamma, \rho)$/Fig. 4(b)	
(2,0.1,0.1,5,5)	A	(2, 0, 0.1, 5, 5)	$A \cup B \cup C \cup D \cup E$
(3,0.1,0.1,5,5)	$A \cup B$	(2, 1, 0.1, 5, 5)	$A \cup B \cup C \cup D$
(4,0.1,0.1,5,5)	$A \cup B \cup C$	(2, 2.5, 0.1, 5, 5)	$A \cup B \cup C$
(5,0.1,0.1,5,5)	$A \cup B \cup C \cup D$	(2, 5, 0.1, 5, 5)	$A \cup B$
(6,0.1,0.1,5,5)	$A \cup B \cup C \cup D \cup E$	(2, 10, 0.1, 5, 5)	A
$(d, d_u, \boldsymbol{d_v}, \gamma, \rho)$/Fig. 4(c)		$(d, d_u, d_v, \boldsymbol{\gamma}, \rho)$/Fig. 4(d)	
(2,0.1,0,5,5)	A	(2, 0.1, 0.1, 2.5, 5)	$A \cup B \cup C \cup D \cup E$
(2,0.1,0.5,5,5)	$A \cup B$	(2, 0.1, 0.1, 3, 5)	$A \cup B \cup C \cup D$
(2,0.1,1,5,5)	$A \cup B \cup C$	(2, 0.1, 0.1, 3.5, 5)	$A \cup B \cup C$
(2,0.1,1.5,5,5)	$A \cup B \cup C \cup D$	(2, 0.1, 0.1, 4, 5)	$A \cup B$
(2,0.1,2,5,5)	$A \cup B \cup C \cup D \cup E$	(2, 0.1, 0.1, 5, 5)	A

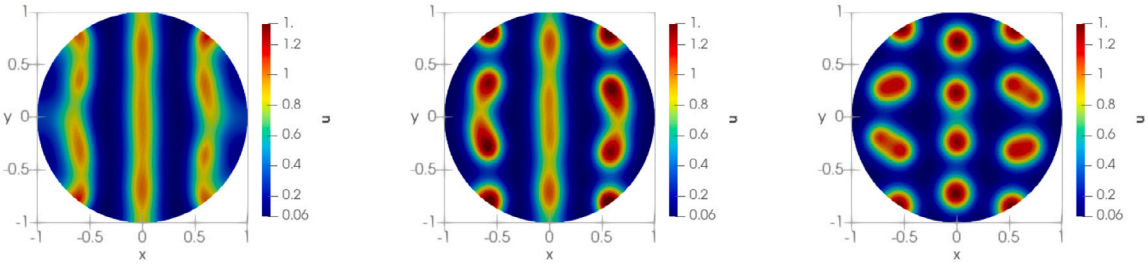

(a) t=0.03 (b) t=0.05 (c) t=0.1

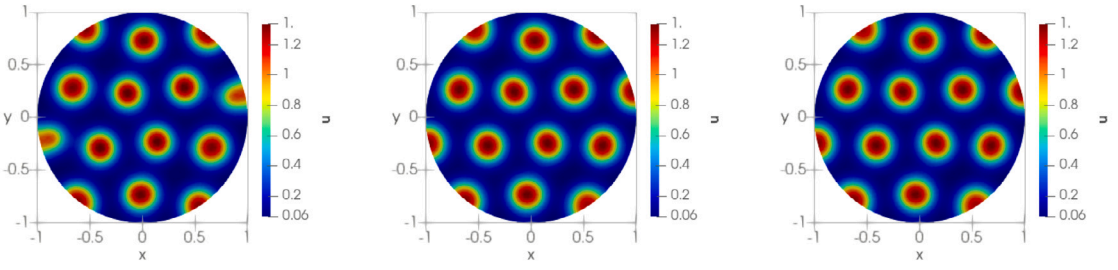

(d) t=0.25 (e) t=1 (f) t=2

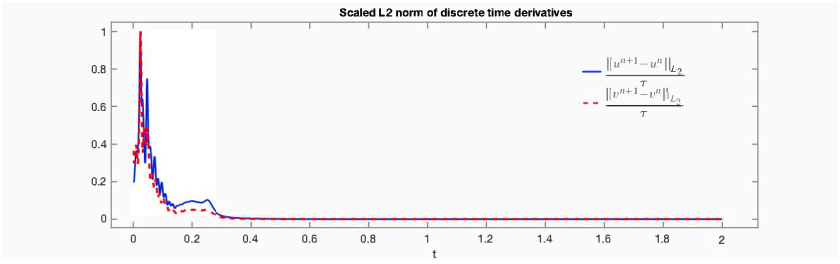

(g) Plot of the L_2 norms of the discrete time derivatives of the numerical solutions u and v.

Fig. 5. (a)–(f) Finite element simulations corresponding to the u-component of the cross-diffusive reaction–diffusion system on a disc-shape domain. Parameters are selected to satisfy conditions of Theorems 2 and 5 with $d = 3.5$, $\gamma = 500$, $d_u = 0.01$, $d_v = 0.85$, $\alpha = 0.1$ and $\beta = 0.3$, as shown in Fig. 3. (g) Plot of the L_2 norms showing the convergence of the numerical solutions u and v.

absence of cross-diffusion. It has been shown in [12] that the case of $d = 1$ cannot give rise to the formation of patterns in the absence of cross-diffusion. Simulations are presented based on the choice of parameters from regions given by Fig. 3 to validate the conditions of Theorems 2 and 5.

In Fig. 7, we demonstrate the evolution of spatial pattern formation corresponding to the choice of model parameters from Turing regions shown in Fig. 4. We note that, the condition on the domain size ρ satisfies Theorem (24) which entails that the only admissible pattern is restricted to Turing type, forbidding the existence of spatiotemporal patterning in the dynamics. Snapshot series illustrated in Fig. 7, showing the development of the u component, exhibit the spatiotemporal dynamics starting with the formation of stripe and spot patterns which transient to form spatially inhomogeneous spot patterns. The plot of the discrete L_2 norms of the discrete time derivative of the numerical solutions u and v, indicate the evolution of the temporal stability dynamics as predicted by condition (24) of Theorem 3.

4.2. Spatiotemporal pattern formation

In this section, we extend our finite element simulations to investigate the effects of parameter selection for the spatiotemporal pattern formation in light of the conditions on the size of disc radius ρ. The choice of the model parameters corresponding to the theoretical predictions are presented in the captions of each figure. We have provided our simulations in a series of snapshots at specific time stages. For each simulation, we provide the plots of the discrete L_2 norm of the discrete time derivative of the numerical solutions of u and v showing the temporal periodicity in the dynamics.

In Fig. 8, we present the finite element simulations when model parameters are selected from the parameter spaces shown in Fig. 2. These correspond to the case when eigenvalues are a complex-conjugate pair. As predicted by the conditions of Theorems 2

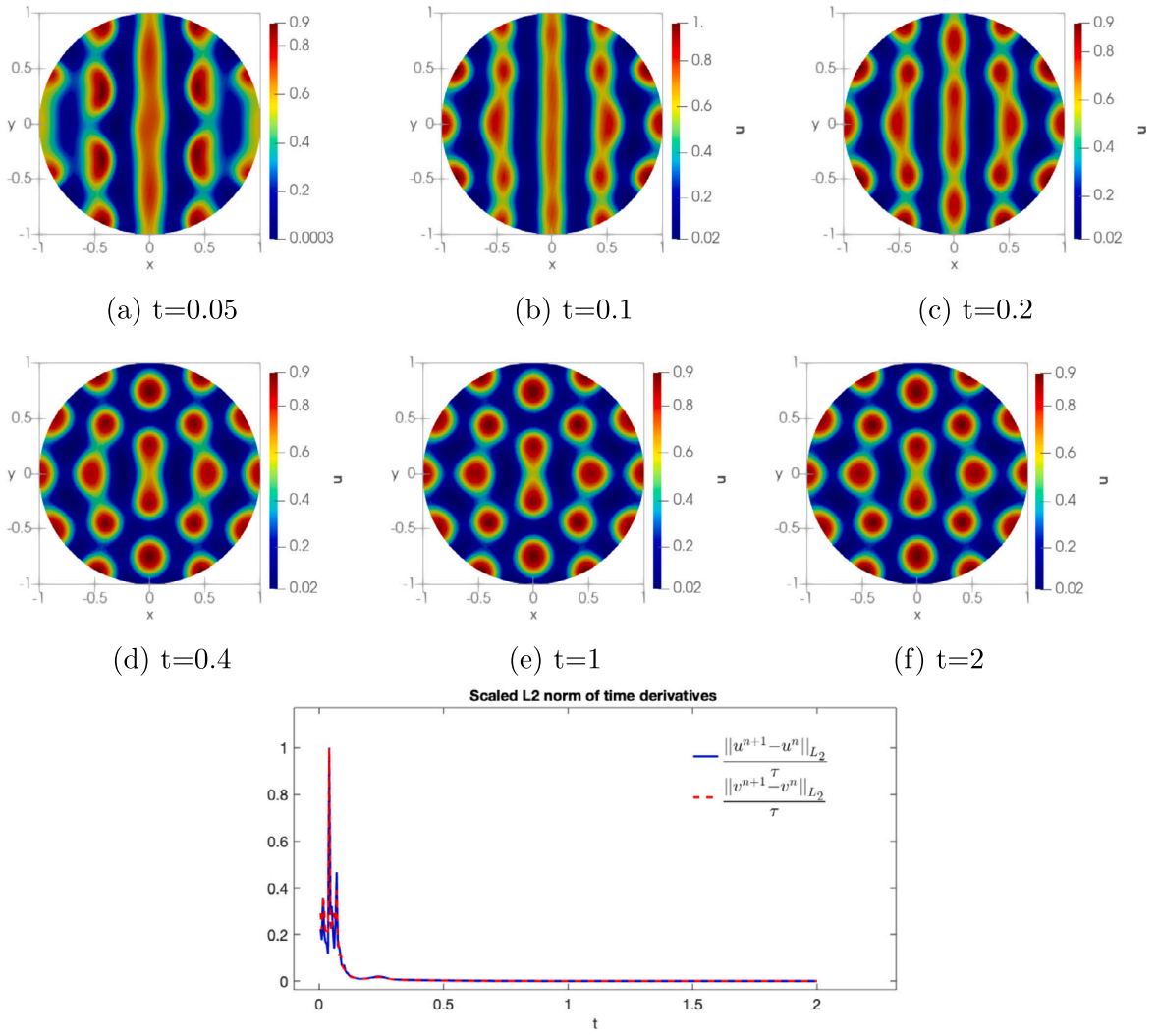

(g) Plot of the L_2 norms of the discrete time derivatives of the numerical solutions u and v

Fig. 6. (a)–(f) Finite element simulations corresponding to the u-component of the cross-diffusive reaction–diffusion system on the disc-shape domain. Parameters are selected to satisfy conditions of Theorems 2 and 5 with $d = 1$, $\gamma = 480$, $d_u = -0.5$, $d_v = 0.43$, $\alpha = 0.07$ and $\beta = 0.3$ as shown in Fig. 3. (g) Plot of the L_2 norms showing the convergence of the numerical solutions u and v.

and 5, time periodicity in the dynamics can be well-observed in the snapshots of Fig. 8. We observe the transition of spot patterns changing from one type to another, periodically. We observe that the periodic spatiotemporal evolution of the spot patterns exhibit a cyclic behaviour in the dynamics of the spot patterns on the circular domain. The L_2 norm of the discrete time derivative of the numerical solutions supports the time periodicity in the short and long term dynamics as shown by Fig. 10 (a) and (b). We also provided a video for this particular simulation as a supplementary material.

Finite element numerical simulations in Fig. 9 are presented to investigate the special case when $d = 1$, which is now able to generate the emergence of patterns only in the presence of cross diffusion. The plot of the L_2 norm of the discrete time derivative of the numerical solutions u and v exhibits the spatiotemporal periodicity, with the same frequency of periodicity and a decaying amplitude, as shown in Fig. 11 (a) and (b). Initially, spot patterns alternate from one form to another, with the system finally converging to inhomogeneous solutions in the long term. The parameters α and β are chosen from the Hopf bifurcation region as shown in Fig. 2.

We demonstrate the effect of negative cross-diffusion in the spatiotemporal pattern formation with a series of snapshots given in Fig. 12. In this particular simulation model parameters are selected as $d = 1$, $d_u = -0.1$, $d_v = 0.5$, $\alpha = 0.085$, in light of Fig. 2 (a)–(b). These correspond to the case when eigenvalues are a complex-conjugate pair. The plot of the L_2 norm of the discrete time derivative of the solutions u and v exhibits spatiotemporal periodicity, with the same frequency of periodicity and amplitude, as shown in Fig. 13 (a) and (b). Spot patterns alternate from one form to another, indicating a limit cycle behaviour in the spatiotemporal dynamics.

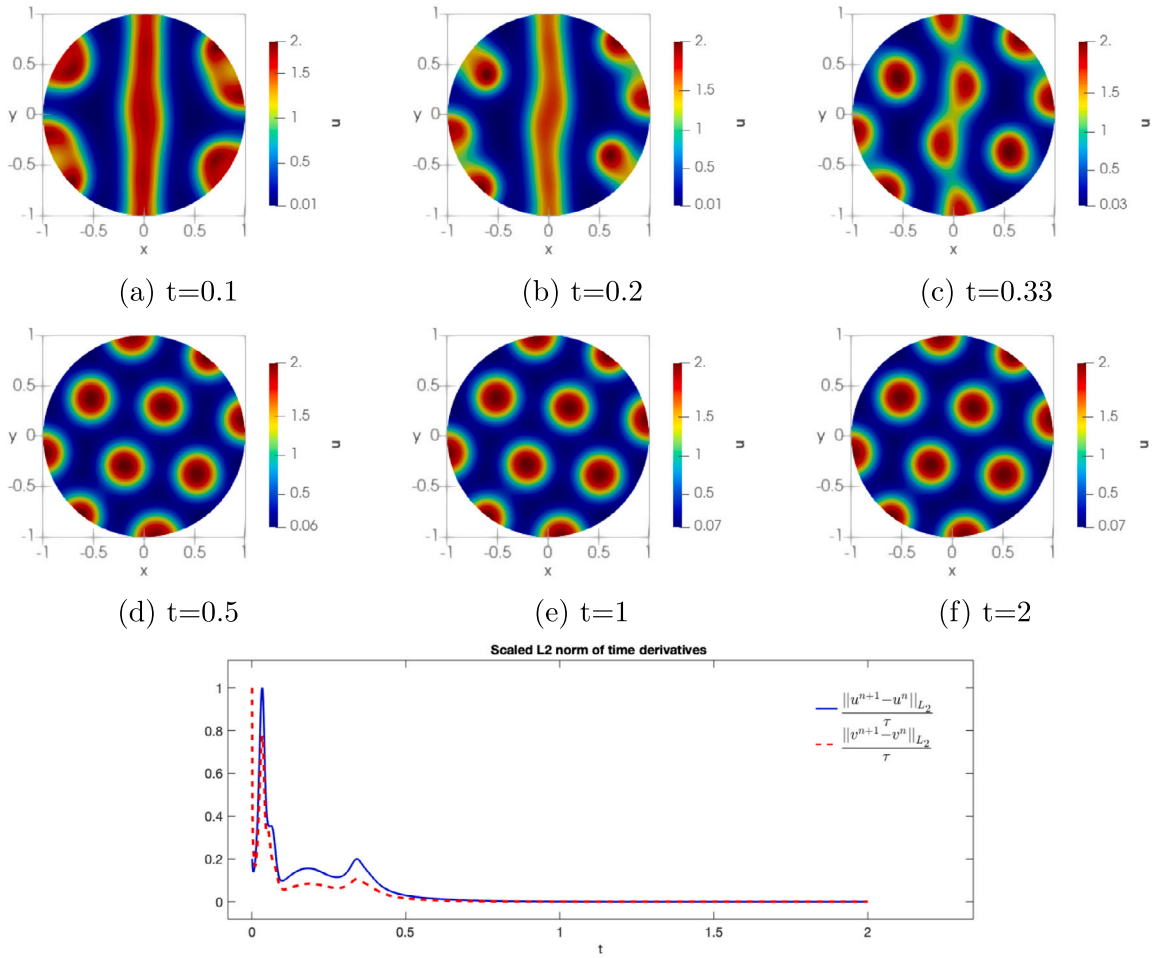

Fig. 7. (a)–(f) Finite element simulations corresponding to the u-component of the cross-diffusive reaction–diffusion system on the disc-shape domain. Parameters are selected to satisfy conditions of Theorems 3 and 5 with $d = 12$, $\gamma = 250$, $d_u = 2$, $d_v = 1$, $\alpha = 0.05$ and $\beta = 0.7$, as shown in Fig. 4. (g) Plot of the L_2 norms showing the convergence of the numerical solutions u and v.

Mathematical analysis of such limit cycles for these types of models (for partial differential equations with linear cross-diffusion) is an open problem.

5. Conclusion

Rigorous mathematical analysis of a cross-diffusive reaction–diffusion model relating the domain-size of the disc with the system parameters is presented for the system exhibiting spatiotemporal pattern formation. An analytical method is employed to derive the conditions on radius of disc ρ. The eigenvalue problem on the disc, whose solution is obtained with the use of Bessel series, plays an essential role in completing the linear stability analysis which is necessary to derive the conditions analytically. Parameter spaces are classified and presented numerically according to conditions of Hopf and transcritical bifurcations, and Turing cross-diffusion-driven instabilities. By using finite element simulations, we demonstrate the existence of spatiotemporal periodicity corresponding to Hopf and transcritical type of bifurcations on a disc shape domain. Our most revealing results show the ability of cross-diffusion as a model candidate to enhance patterning when coupled with the classical self-diffusion process. The inclusion of linear cross-diffusion entails that equal self-diffusion coefficients are able to give rise to spatial pattern formation, which is not possible if cross-diffusion is not present as a physical process. Such novel results entail the relaxation of the restrictive Turing diffusion-driven instability conditions.

Some of the open problems in this area include (but are not limited to):

- Stability analysis of reaction–diffusion systems with linear cross-diffusion on growing domains and evolving surfaces.

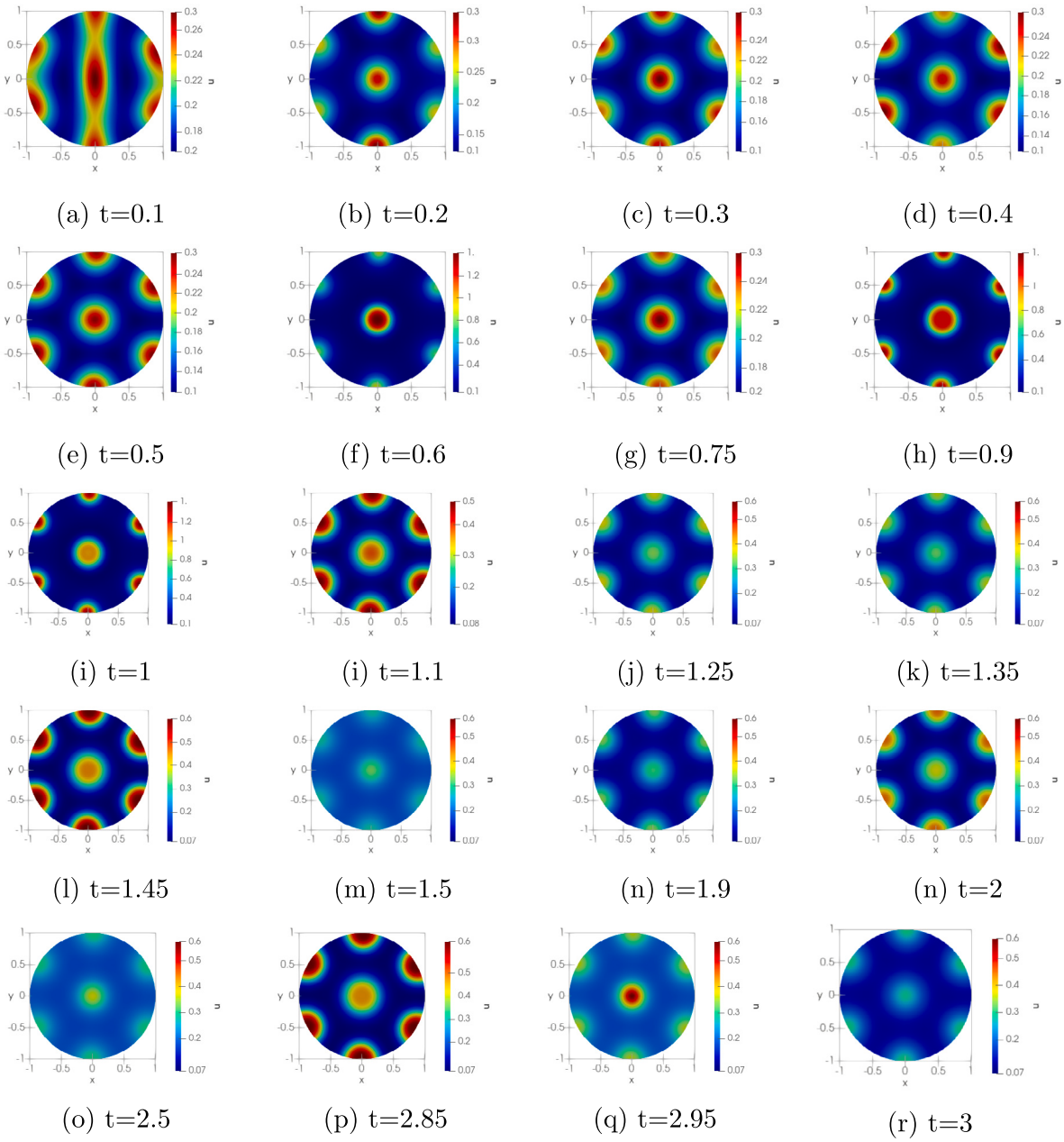

Fig. 8. Finite element simulations corresponding to the u-component of the cross-diffusive reaction–diffusion system on the disc shape domain exhibiting spatiotemporal pattern formation. Parameters are selected to satisfy conditions of Theorems 2 and 5 on ρ with $d = 2.6$, $\gamma = 375$, $d_u = 1$, $d_v = 0.65$, $\alpha = 0.09$ and $\beta = 0.1$, as shown in Fig. 2.

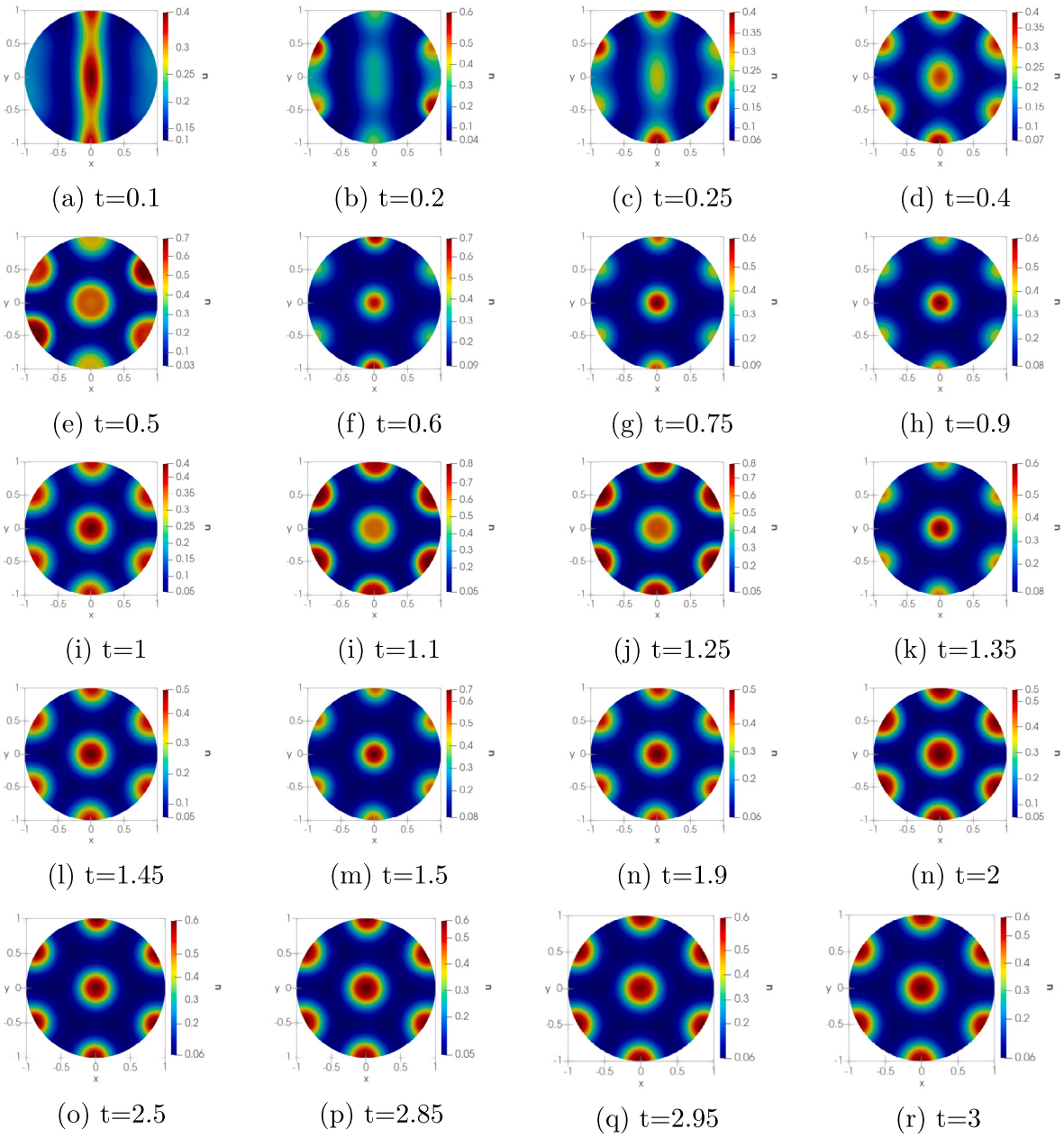

Fig. 9. Finite element simulations corresponding to the u-component of the cross-diffusive reaction–diffusion system on the disc shape domain exhibiting spatiotemporal pattern formation. Parameters are selected to satisfy conditions of Theorems 2 and 5 on ρ with $d = 1$, $\gamma = 180$, $d_u = 0.5$, $d_v = 0.5$, $\alpha = 0.085$ and $\beta = 0.1$.

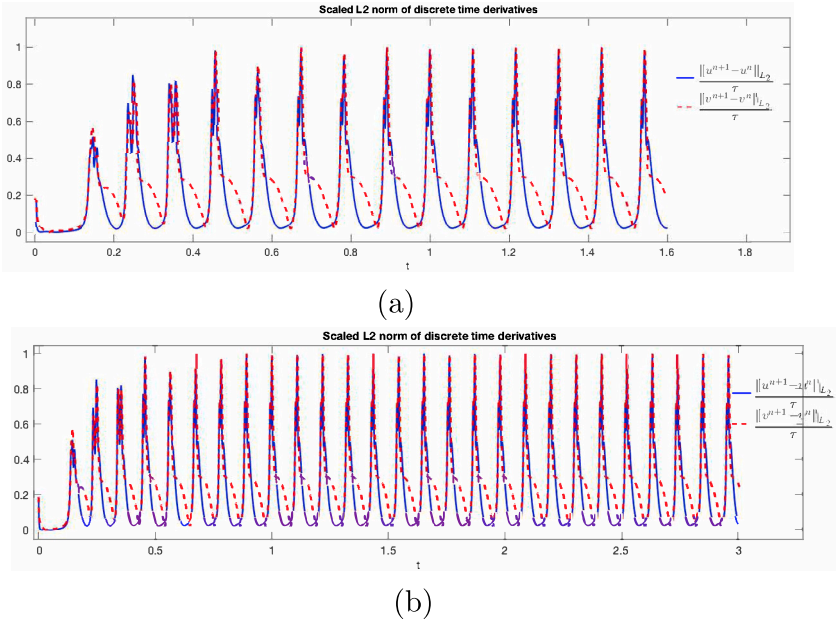

Fig. 10. (a) The plot of the discrete time derivative of the numerical solutions u and v showing the spatiotemporal periodicity on $t \in [0, 1.6]$ for the numerical simulation shown in Fig. 8. (b) The plot of the discrete time derivative of the numerical solutions u and v showing the spatiotemporal periodicity on $t \in [0, 3]$ for the numerical simulation shown in Fig. 8.

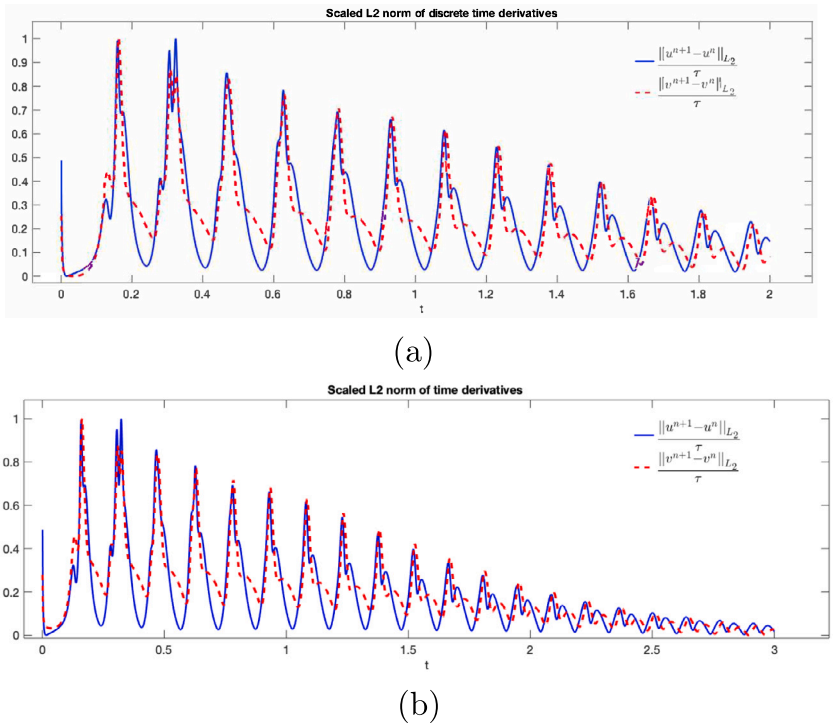

Fig. 11. (a) The plot of the discrete time derivative of the numerical solutions u and v showing the spatiotemporal periodicity for $t \in [0, 2]$ of the numerical simulation shown in Fig. 9. (b) The plot of the discrete time derivative of the numerical solutions u and v showing the spatiotemporal periodicity on $t \in [0, 3]$ for the numerical simulation shown in Fig. 9.

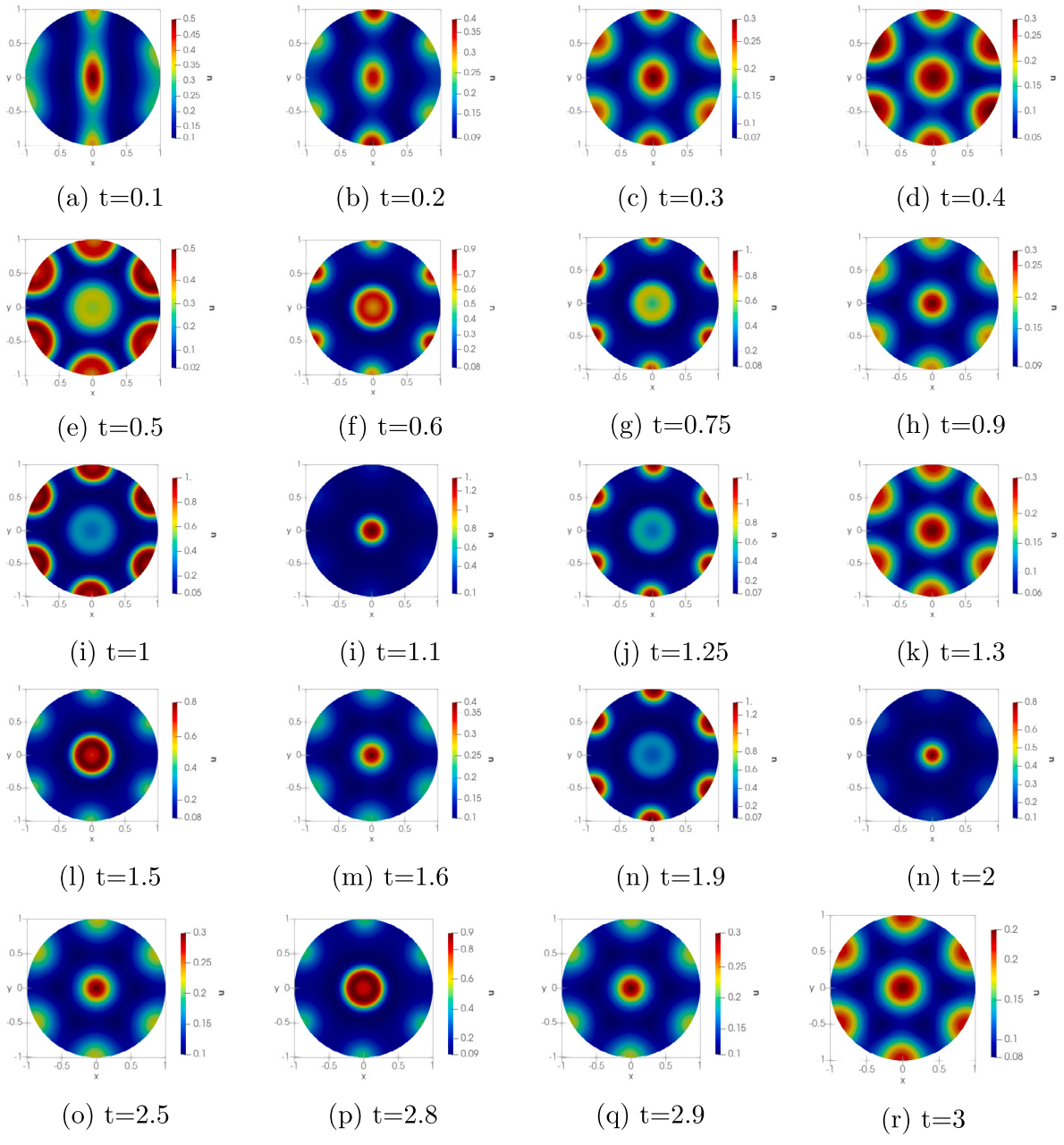

Fig. 12. Finite element simulations corresponding to the u-component of the reaction–diffusion system on the disc shape domain exhibiting spatiotemporal pattern formation with negative cross-diffusion. Parameters are selected to satisfy conditions of Theorems 2 and 5 on ρ with $d = 1$, $\gamma = 250$, $d_u = -0.1$, $d_v = 0.5$, $\alpha = 0.085$ and $\beta = 0.1$.

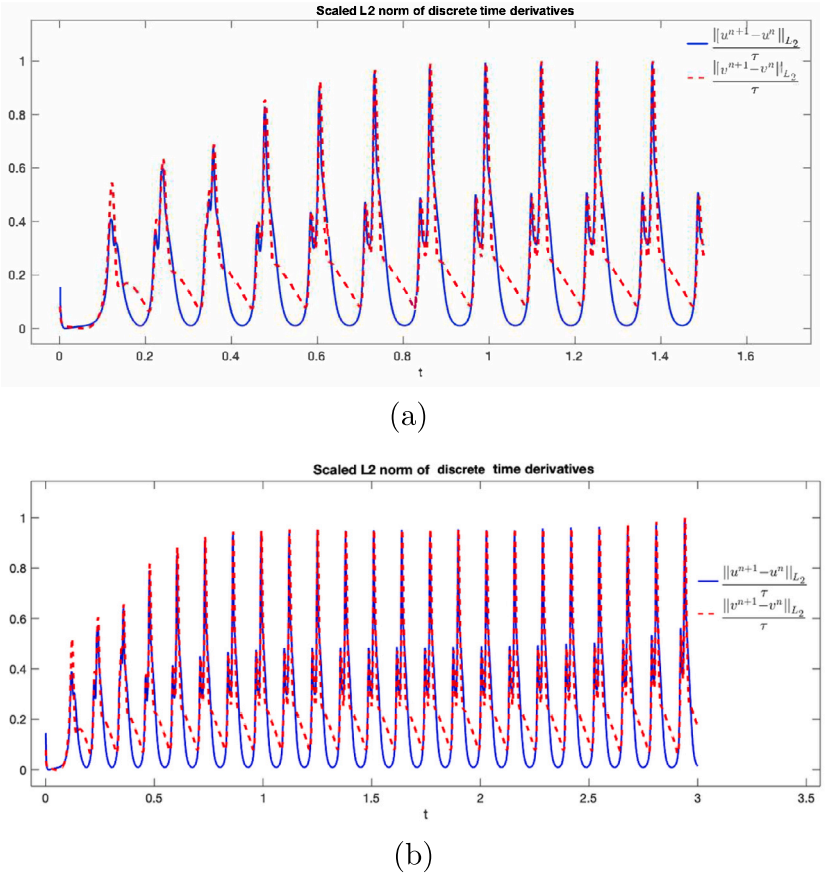

Fig. 13. (a) The plot of the discrete time derivative of the numerical solutions u and v showing the spatiotemporal periodicity on $t \in [0, 1.6]$ for the numerical simulation shown in Fig. 12. (b) The plot of the discrete time derivative of the numerical solutions u and v showing the spatiotemporal periodicity on $t \in [0, 3]$ for the numerical simulation shown in Fig. 12.

- Bifurcation analysis of semi-linear parabolic systems of reaction–diffusion equations with linear cross-diffusion to study the transitions from uniform states to limit cycles.
- Stability analysis of reaction–diffusion systems with nonlinear cross-diffusion. Solution methods for such systems could include perturbation theory involving weakly nonlinear analysis for partial differential equations.
- Stability analysis of multi-component reaction–diffusion systems with linear cross-diffusion.

These open problems form part of our current studies.

CRediT authorship contribution statement

Gulsemay Yigit: Conceptualization, Formal analysis, Investigation, Methodology, Numerical Simulations, Software, Validation, Writing – original draft, Editing, Review. **Wakil Sarfaraz:** Conceptualization, Formal analysis, Investigation, Methodology, Review, Editing, Funding acquisition. **Raquel Barreira:** Data curation, Numerical Simulations, Software, Writing – review & editing. **Anotida Madzvamuse:** Conceptualisation, Project administration, Formal analysis, Investigation, Methodology, Resources, Supervision, Validation, Visualization, Writing – review & editing, Funding acquisition.

Acknowledgements

AM is a Canada Research Chair (Tier 1) in Theoretical and Computational Biology (CRC-2022-00147). This work (AM) was partially supported by the Natural Sciences and Engineering Research Council of Canada (NSERC), Discovery Grants Program (RGPIN-2023-05231), and the Engineering and Physical Sciences Research Council, United Kingdom (EPSRC: EP/J016780/1). AM acknowledges the Royal Society Merit Award (2016–2021) funded generously by the Wolfson Foundation, United Kingdom. This work (AM, GY, RB) was partially carried out while AM, GY and RB were at the International Center for Mathematical Sciences (ICMS) in Edinburgh for the Research in Group Meeting (1st–10th September 2022). RB was partially supported by National Funding from

FCT — Fundação para a Ciência e Tecnologia, Portugal, under the project UIDB/04561/2020. WS acknowledges the support from UBC Mathematics Department start-up fund grant (awarded to AM) for open-source publication costs of the article. The authors acknowledge the significant contributions of the reviewers, their comments helped to improve the quality of the manuscript.

Appendix A. Supplementary data

Supplementary material related to this article can be found online at https://doi.org/10.1016/j.nonrwa.2023.104042.

References

[1] J.D. Murray, Mathematical Biology II: Spatial Models and Biomedical Applications, Vol. 3, Springer New York, 2001.
[2] R.E. Baker, E. Gaffney, P. Maini, Partial differential equations for self-organization in cellular and developmental biology, Nonlinearity 21 (11) (2008) R251.
[3] A. Gierer, H. Meinhardt, a theory of biological pattern formation, Kybernetic 12 (1972) 30–39.
[4] R.A. Satnoianu, M. Menzinger, P.K. Maini, Turing instabilities in general systems, J. Math. Biol. 41 (2000) 493–512.
[5] A. Madzvamuse, A Numerical Approach to the Study of Spatial Pattern Formation (Ph.D. thesis), University of Oxford, 2000.
[6] R.A. Barrio, R.E. Baker, B. Vaughan Jr., K. Tribuzy, M.R. de Carvalho, R. Bassanezi, P.K. Maini, Modeling the skin pattern of fishes, Phys. Rev. E 79 (3) (2009) 031908.
[7] A.M. Turing, The chemical basis of morphogenesis, Bull. Math. Biol. 52 (1–2) (1990) 153–197.
[8] V.K. Vanag, I.R. Epstein, Pattern formation mechanisms in reaction-diffusion systems, Int. J. Dev. Biol. 53 (5–6) (2009) 673–681.
[9] V.K. Vanag, I.R. Epstein, Cross-diffusion and pattern formation in reaction–diffusion systems, Phys. Chem. Chem. Phys. 11 (6) (2009) 897–912.
[10] R. Barreira, C.M. Elliott, A. Madzvamuse, The surface finite element method for pattern formation on evolving biological surfaces, J. Math. Biol. 63 (2011) 1095–1119.
[11] A. Madzvamuse, H.S. Ndakwo, R. Barreira, Cross-diffusion-driven instability for reaction-diffusion systems: analysis and simulations, J. Math. Biol. 70 (4) (2015) 709–743.
[12] A. Madzvamuse, H. Ndakwo, R. Barreira, Stability analysis of reaction-diffusion models on evolving domains: the effects of cross-diffusion, Discrete Contin. Dyn. Syst. 36 (4) (2015) 2133–2170.
[13] A. Madzvamuse, A.H. Chung, C. Venkataraman, Stability analysis and simulations of coupled bulk-surface reaction–diffusion systems, Proc. R. Soc. Lond. Ser. A Math. Phys. Eng. Sci. 471 (2175) (2015) 20140546.
[14] J. Schnakenberg, Simple chemical reaction systems with limit cycle behaviour, J. Theoret. Biol. 81 (3) (1979) 389–400.
[15] W. Sarfaraz, A. Madzvamuse, Classification of parameter spaces for a reaction-diffusion model on stationary domains, Chaos Solitons Fractals 103 (2017) 33–51.
[16] W. Sarfaraz, A. Madzvamuse, Domain-dependent stability analysis of a reaction–diffusion model on compact circular geometries, Int. J. Bifurcation Chaos 28 (08) (2018) 1830024.
[17] W. Sarfaraz, A. Madzvamuse, Stability analysis and parameter classification of a reaction–diffusion model on an annulus, J. Appl. Nonlinear Dyn. 9 (4) (2020) 589–617.
[18] E.P. Zemskov, V.K. Vanag, I.R. Epstein, Amplitude equations for reaction-diffusion systems with cross diffusion, Phys. Rev. E 84 (3) (2011) 036216.
[19] Q. Li, Z. Liu, S. Yuan, Cross-diffusion induced turing instability for a competition model with saturation effect, Appl. Math. Comput. 347 (2019) 64–77.
[20] J.-F. Zhang, H.-B. Shi, A. Madzvamuse, Characterizing the effects of self-and cross-diffusion on stationary patterns of a predator–prey system, Int. J. Bifurcation Chaos 30 (03) (2020) 2050041.
[21] M. Song, S. Gao, C. Liu, Y. Bai, L. Zhang, B. Xie, L. Chang, Cross-diffusion induced turing patterns on multiplex networks of a predator–prey model, Chaos Solitons Fractals 168 (2023) 113131.
[22] W. Yang, Y. Maimaiti, Cross-diffusion-driven instability and pattern formation in a nonlinear predator-prey system, IAENG Int. J. Appl. Math. 53 (1) (2023) 1–5.
[23] F. Yi, Turing instability of the periodic solutions for reaction-diffusion systems with cross-diffusion and the patch model with cross-diffusion-like coupling, J. Differential Equations 281 (2021) 379–410.
[24] R. Kersner, M. Klincsik, D. Zhanuzakova, A competition system with nonlinear cross-diffusion: exact periodic patterns, Rev. Real Acad. Cienc. Exact. Físic. Nat. Ser. A Mat. 116 (4) (2022) 187.
[25] J.S. Ritchie, A.L. Krause, R.A. Van Gorder, Turing and wave instabilities in hyperbolic reaction–diffusion systems: The role of second-order time derivatives and cross-diffusion terms on pattern formation, Ann. Phys. 444 (2022) 169033.
[26] S. Kumari, S.K. Tiwari, R.K. Upadhyay, Cross diffusion induced spatiotemporal pattern in diffusive nutrient–plankton model with nutrient recycling, Math. Comput. Simulation 202 (2022) 246–272.
[27] R. Yang, Cross-diffusion induced spatiotemporal patterns in Schnakenberg reaction–diffusion model, Nonlinear Dynam. 110 (2) (2022) 1753–1766.
[28] H. Liu, B. Ge, J. Shen, Dynamics of periodic solutions in the reaction-diffusion glycolysis model: Mathematical mechanisms of turing pattern formation, Appl. Math. Comput. 431 (2022) 127324.
[29] N. Bellomo, N. Outada, J. Soler, Y. Tao, M. Winkler, Chemotaxis and cross-diffusion models in complex environments: models and analytic problems toward a multiscale vision, Math. Models Methods Appl. Sci. 32 (04) (2022) 713–792.
[30] Y.-J. Kim, C. Yoon, Modeling bacterial traveling wave patterns with exact cross-diffusion and population growth, Discrete Contin. Dyn. Syst. Ser. B (2023).
[31] E.A. Gaffney, A.L. Krause, P.K. Maini, C. Wang, Spatial heterogeneity localizes turing patterns in reaction-cross-diffusion systems, 2022, arXiv preprint arXiv:2210.10155.
[32] M. Duan, L. Chang, Z. Jin, Turing patterns of an SI epidemic model with cross-diffusion on complex networks, Physica A 533 (2019) 122023.
[33] L. Chang, M. Duan, G. Sun, Z. Jin, Cross-diffusion-induced patterns in an SIR epidemic model on complex networks, Chaos 30 (1) (2020) 013147.
[34] J. Hu, L. Zhu, Turing pattern analysis of a reaction-diffusion rumor propagation system with time delay in both network and non-network environments, Chaos Solitons Fractals 153 (2021) 111542.
[35] N. Mohan, N. Kumari, Positive steady states of a SI epidemic model with cross diffusion, Appl. Math. Comput. 410 (2021) 126423.
[36] D. Lacitignola, B. Bozzini, R. Peipmann, I. Sgura, Cross-diffusion effects on a morphochemical model for electrodeposition, Appl. Math. Model. 57 (2018) 492–513.
[37] A.L. Krause, M.A. Ellis, R.A. Van Gorder, Influence of curvature, growth, and anisotropy on the evolution of turing patterns on growing manifolds, Bull. Math. Biol. 81 (2019) 759–799.
[38] M. Frittelli, I. Sgura, Matrix-oriented FEM formulation for reaction-diffusion PDEs on a large class of 2D domains, Appl. Numer. Math. (2023).
[39] D. Lacitignola, B. Bozzini, M. Frittelli, I. Sgura, Turing pattern formation on the sphere for a morphochemical reaction-diffusion model for electrodeposition, Commun. Nonlinear Sci. Numer. Simul. 48 (2017) 484–508.

[40] A. Madzvamuse, P.K. Maini, Velocity-induced numerical solutions of reaction-diffusion systems on continuously growing domains, J. Comput. Phys. 225 (1) (2007) 100–119.
[41] A. Madzvamuse, A.H. Chung, Fully implicit time-stepping schemes and non-linear solvers for systems of reaction–diffusion equations, Appl. Math. Comput. 244 (2014) 361–374.
[42] O. Lakkis, A. Madzvamuse, C. Venkataraman, Implicit–explicit timestepping with finite element approximation of reaction–diffusion systems on evolving domains, SIAM J. Numer. Anal. 51 (4) (2013) 2309–2330.
[43] N. Tuncer, A. Madzvamuse, Projected finite elements for systems of reaction-diffusion equations on closed evolving spheroidal surfaces, Commun. Comput. Phys. 21 (3) (2017) 718–747.
[44] M. Frittelli, A. Madzvamuse, I. Sgura, Bulk-surface virtual element method for systems of PDEs in two-space dimensions, Numer. Math. 147 (2) (2021) 305–348.
[45] J. Smoller, Shock Waves and Reaction—Diffusion Equations, Vol. 258, Springer Science & Business Media, 2012.
[46] L. Qi, Y. Song, X. Zhang, Positivity conditions for cubic, quartic and quintic polynomials, 2020, arXiv preprint arXiv:2008.10922.
[47] J.W. Schmidt, W. Heß, Positivity of cubic polynomials on intervals and positive spline interpolation, BIT Numer. Math. 28 (1988) 340–352.
[48] A. Madzvamuse, R. Barreira, Exhibiting cross-diffusion-induced patterns for reaction-diffusion systems on evolving domains and surfaces, Phys. Rev. E 90 (4) (2014) 043307.
[49] L.C. Evans, Partial Differential Equations, Vol. 19, American Mathematical Society, 2022.
[50] S.C. Brenner, L.R. Scott, The Mathematical Theory of Finite Element Methods, Springer, 2008.
[51] C. Geuzaine, J.-F. Remacle, Gmsh: A 3-D finite element mesh generator with built-in pre-and post-processing facilities, Internat. J. Numer. Methods Engrg. 79 (11) (2009) 1309–1331.
[52] A. Madzvamuse, Time-stepping schemes for moving grid finite elements applied to reaction–diffusion systems on fixed and growing domains, J. Comput. Phys. 214 (1) (2006) 239–263.
[53] S.J. Ruuth, Implicit-explicit methods for reaction-diffusion problems in pattern formation, J. Math. Biol. 34 (2) (1995) 148–176.
[54] A. Madzvamuse, A modified backward Euler scheme for advection-reaction-diffusion systems, in: Mathematical Modeling of Biological Systems, Volume I: Cellular Biophysics, Regulatory Networks, Development, Biomedicine, and Data Analysis, Springer, 2007, pp. 183–189.